Schweizerische Eidgenossenschaft
Confédération suisse
Confederazione Svizzera
Confederaziun svizra

Department of the Environment,
Transport, Energy and Communication DETEC

**Swiss Federal Office of Energy SFOE**
Energy Research

**Annual report from 10 May 2023**

---

# ODIS

## Optimal DSO dISpatchability

---

University of Applied Sciences and Arts
of Southern Switzerland

SUPSI

**Date:** 10 May 2023

**Place:** Bern

**Publisher:**
Swiss Federal Office of Energy SFOE
Research Programme, Grid
CH-3003 Bern
www.bfe.admin.ch
energieforschung@bfe.admin.ch

**Author:**
Lorenzo Nespoli, ISAAC, SUPSI (lorenzo.nespoli@supsi.ch)
Jalomi Maayan Tardif, ISAAC, SUPSI (jalomi.maayantardif@supsi.ch)
Matteo Palucci, ISAAC, SUPSI (matteo.palucci@supsi.ch)
Vasco Medici, ISAAC, SUPSI (vasco.medici@supsi.ch)
Roman Rudel, ISAAC, SUPSI (roman.rudel@supsi.ch)

**SFOE head of domain:** Dr. Michael Moser, michael.moser@bfe.admin.ch
**SFOE programme manager:** Dr. Michael Moser, michael.moser@bfe.admin.ch
**SFOE contract number:** SI/502074

# Summary

Distribution networks are rapidly becoming "active", as accurate control over electricity generation sources and loads make them partially dispatchable. This flexibility, when correctly identified and aggregated, could be used by the Distribution System Operators (DSO) to optimize local grid efficiency and, if possible, to offer services to third parties, thereby providing an additional revenue stream. Furthermore, correctly quantifying the available flexibility would enable an equitable exchange of energy data and could expand the conventional and currently restricted exchanges between customer, the DSO and the Transmission System Operator (TSO).

This project aims to develop a general but practical dynamic flexibility model that helps the DSO make informed decisions on optimally controlling its flexibility to reach a techno-economic optimum. At first, a mechanism to assess the impact of flexibility actuation on the DSO load curve, which can estimate the amount of flexibility from day zero without relying on historical observations, is presented. We achieve this by simulating the flexible devices, starting from publicly available metadata, and learning their response to a random control signal using a non-parametric global forecasting model. This forecasting model can be used to characterize flexibility, including rebound effects, answering questions such as: how the controlled device mix influences flexibility? How many kWh, at which power level, could be deferred? This model is then used to define an optimal control policy that can be used to maximize the savings of the DSO. A method to control heat pumps without violating the end-users' thermal comfort, relying on the estimation of the energy signature for the controlled buildings, is presented and integrated in the control loop. We then show how we can estimate the cost-saving potential under different penetration scenarios for the controlled devices for the use case of a specific DSO. In the considered case study of the Azienda Multiservizi di Bellinzona, the data-driven forecaster estimated an annual cost reduction of 640 kCHF, equivalent to a reduction of the overall energy and peak expenses of about 1.4 %, under the participation of the maximum considered penetration of heat pumps and electric heaters.

Secondly, we propose a long-term scenario assessment of the evolution and impact of flexibility in the distribution grid based on a System Dynamics approach. This model can be used to estimate the evolution of the cost-saving potential, its impact on the penetration of flexible devices, and future economic benefits for the end users. A replicability analysis of the methodology is proposed on a second use-case, using data from the Services industriels de Genève (SIG).

A potential way to ensure scalability could be to seek not only savings derived from the DSO-TSO energy and peak power tariff scheme but also revenues by offering the aggregated flexibility to third parties or directly accessing ancillary markets, and including other energivouros devices in the control loop.



# Sommario

Le reti di distribuzione stanno rapidamente diventando "attive", ed un controllo accurato delle fonti di generazione elettrica e dei carichi le rende parzialmente dispacciabili. Questa flessibilità, se correttamente identificata e aggregata, potrebbe essere utilizzata dai gestori dei sistemi di distribuzione o trasmissione per ottimizzare l'efficienza della rete locale e, se possibile, per offrire servizi a terzi, fornendo così un ulteriore flusso di entrate. Inoltre, la corretta quantificazione della flessibilità disponibile consentirebbe uno scambio di dati energetici e potrebbe ampliare gli scambi convenzionali e attualmente limitati tra cliente, gestori di distribuzione e gestori di trasmissione.

Questo progetto mira a sviluppare un modello di flessibilità dinamica generale ma pratico, che aiuti il gestore di distribuzione a prendere decisioni informate sul controllo ottimale della propria flessibilità per

raggiungere un optimum tecno-economico. In primo luogo, viene presentato un meccanismo per valutare l'impatto dell'attivazione della flessibilità sulla curva di carico del gestore di distribuzione, in grado di stimare la quantità di flessibilità a partire dal giorno zero senza basarsi su osservazioni storiche. Per ottenere questo risultato, abbiamo simulato i dispositivi flessibili, partendo da metadati pubblicamente disponibili, imparando la loro risposta a un segnale di controllo casuale utilizzando un modello di previsione globale non parametrico. Questo modello di previsione può essere utilizzato per caratterizzare la flessibilità, compresi gli effetti di rebound, rispondendo a domande quali: come il mix di dispositivi controllati influisce sulla flessibilità? Quanti kWh, a quale livello di potenza, possono essere spostati? Questo modello viene poi utilizzato per definire una politica di controllo ottimale che può essere utilizzata per massimizzare i risparmi del DSO. Viene presentato un metodo per controllare le pompe di calore senza violare il comfort termico degli utenti finali, basato sulla stima della firma energetica degli edifici controllati e integrato nel circuito di controllo. Mostriamo poi come sia possibile stimare il potenziale di risparmio dei costi in diversi scenari di penetrazione dei dispositivi controllati per il caso d'uso di uno specifico DSO. Nel caso di studio considerato dell'Azienda Multiservizi di Bellinzona, il previsore ha stimato una riduzione dei costi annuali di 640 kCHF, equivalente a una riduzione delle spese complessive per l'energia e dei picchi di circa l'1,4 %, nel caso di massima penetrazione considerata di pompe di calore e riscaldatori elettrici.

In secondo luogo, proponiamo una valutazione dello scenario a lungo termine dell'evoluzione e dell'impatto della flessibilità nella rete di distribuzione basata su un approccio System Dynamics. Questo modello può essere utilizzato per stimare l'evoluzione del potenziale di risparmio, il suo impatto sulla penetrazione dei dispositivi flessibili e i futuri benefici economici per gli utenti finali. Viene proposta un'analisi di replicabilità della metodologia su un secondo caso d'uso, utilizzando i dati del Services industriels de Genève (SIG).

Un modo per garantire la scalabilità del metodo presentato potrebbe essere quello di ricercare non solo i risparmi derivanti dallo schema tariffario del gestore di distribuzione-trasmissione per l'energia e i picchi di potenza, ma anche i ricavi derivanti dall'offerta della flessibilità aggregata a terzi, e includere nel controllo altri carichi energivori.

# Contents

# List of abbreviations

| | |
|---|---|
| AET | Azienda Elettrica Ticinese |
| AMB | Azienda Multiservizi Bellinzona |
| DER | Distributed Energy Resources |
| DFH | Dual Family House |
| DHW | Domestic Hot Water |
| DR | Demand Response |
| DSO | Distribution System Operator |
| EH | Electric Heating |
| EV | Electric Vehicle |
| HP | Heat Pump |
| HT | Heating Technology |
| MFH | Multi Family House |
| PV | Photovoltaic |
| SD | System Dynamics |
| SFH | Single Familiy House |
| SH | Space Heating |
| ST | Solar Thermal |

# 1 Introduction

Distribution networks are rapidly becoming "active", as accurate control over electricity generation sources and loads make them partially dispatchable. Such flexibility, when correctly identified and aggregated, could be used by the Distribution System Operator (DSO) to optimize local grid efficiency and, if possible, to offer services to third parties, thereby providing an additional revenue stream. This project aims to develop a general but practical dynamic flexibility model that helps the DSO to make informed decisions on how optimally control its flexibility, such as to reach a techno-economic optimum.

Our work builds on two different concepts in the field of flexibility studies: simulation-based flexibility assessment and inverse optimization of price signals. The first concept has been explored in [1], where authors assessed the energy flexibility potential of a pool of residential smart-grid-ready heat pumps (i.e., with an internal controller reacting to a discrete signal indicating if they have to consume more, less or shut down) by means of bottom-up simulations. Other studies tried to assess the energy flexibility of residential buildings using simulations, like [2] and [3]; however, they start from the hypothesis of being able to directly control flexible devices. In particular, in [2], the authors wanted to provide to an aggregator with an index describing the additional energy used for a desired change in power consumption, using simulation and MPC. Unfortunately, the analysis is of little use since this relation also depends on the time of flexibility activation, as pointed out in [4].

Inverse optimization of price signals has been first introduced in [5]. The idea is that it is possible to optimize scheduling of a price signal to optimize the objective of an aggregator, knowing that some sort of price-dependent controller optimizes flexible loads. To show this, authors fit an (invertible) online FIR model to forecast the consumption of a group of buildings as a function of a price signal and derive an analytic solution for an associated closed-loop controller. The concept is then demonstrated by means of simulations on 20 heat-pump-equipped households. The authors of [6] use the same concept presented in [5] to fit a linear model linking prices and the load of a cluster of price-sensitive buildings. The authors then propose to characterize flexibility extracting parameters from the model response. They also propose to estimate the expected saving of a given building by simulating its model twice, with and without a price-reacting control. A similar approach was proposed in [7], where authors identified a general stochastic nonlinear model for the prediction of energy flexibility coming from a water tower operated by an unknown control strategy. The fitted model is then used in an optimization loop to design price signals for the optimal exploitation of flexibility. Authors in [8] used the same method to find price signals to best meet flexibility requests using an iterative method.

The System Dynamics model, whose purpose is to assess the long-term adoption of flexible devices and the share of these that are put at the disposal of the DSO, builds on theories of non-linear dynamics and feedback loops developed in mathematics, physics, and engineering [9] [10] [11]; System Dynamics was chosen for this study as it has been suggested and applied several times for the study of socio-technical transition processes (see [12] for a comprehensive review).

## 1.1 Background information and current situation

As a proof of concept, ODIS focuses on the coordination between the DSO Azienda Multiservizi Bellinzona (AMB) and the Azienda Elettrica Ticinese (AET), which serves as a Transmission System Operator (TSO) for Ticino. During the meetings with the project partners, the following conditions were defined for the proof of concept:

1. The original project proposed to consider grid constraints as a boundary condition to the optimization problem. Since AMB re-wires substations several times for maintenance reasons and these activities cannot be known in advance (nor do records exists of such a process), we shifted the focus from grid constraints to thermal comfort constraints for the end users. This doesn't impact the control methods and approaches developed in the project; grid constraints can be easily considered for other use cases where the information on grid topology and measurements of grid re-configurations are available.

2. Analyzing the different business models with the project partners, we agreed to focus the use case on the day ahead cost optimization and on peak price optimization. The latter is of particular interest for DSO-TSO coordination since this cost is paid by the DSO to the TSO.

## 1.2 Purpose of the project

Coordinated exploitation of flexibilities in the distribution or transmission grid can potentially be used to increase grid resilience, reduce maintenance costs, lower distribution losses, increase the predictability of the demand profile, and shift consumption in the function of tariff structures and energy supply patterns. Yet, this requires the aggregation of flexible customers into "pools" that reach a critical mass. In most cases, aggregation requires control over heterogeneous types of devices, as well as different types of controllers, (e.g., rule or heuristic-based, model predictive control, etc.). Currently, this condition restricts the viable control methods for pooling flexibility to ripple control, a method using frequency-sensitive relays to shut down flexible devices. The other most commonly considered type of control is indirect and uses tariff structures; however, the effectiveness of this second method depends on the capacity and willingness of the asset owner to respond to the signal, either manually or conditional to the presence of smart devices which can optimize energy use based on the price signal, the latter being currently not widespread in most distribution grids. Most often, the activation of flexibility has ripple effects on the load curve following the control action. This "rebound effect" could have negative consequences for the DSOs and collaborating third parties and must be considered during the optimization.

## 1.3 Objectives

We aim to demonstrate a data-driven methodology to characterize and control flexibility in terms of the power system response to a given broadcasted control signal. The aim of the characterization is to obtain an oracle or forecaster able to capture the change in demand in different regions of the grid based on the number and type of flexible loads. This forecaster can then be used to simulate the rebound effect and include this knowledge in an optimization loop. Our objectives can be summarized in the following:

- Simulate flexible loads' response to a ripple control signal using public available data for a given DSO's grid.
- Learn from simulated data a characterization of flexibility (how many kWh can be deferred, with which power, for how long?) through a non-parametric regressor, or oracle, which is able to generalize beyond control action seen during simulations.
- Integrate the regressor into an optimization loop to optimally control available flexibility
- Use this method to estimate the cost-saving potential for a given DSO and generate what-if analysis under different future penetration of flexible and controllable devices.
- Use these economic results as inputs of a System Dynamics model, which can be used to estimate the evolution of the cost-saving potential, its impact on the penetration of flexible devices, and future economic benefits for the end users
- Perform a replicability analysis applying the whole methodology to a different case study

# 2 Procedures and methodology

## 2.1 Modeling and simulation of flexibility

To demonstrate our methodology, we have simulated the available flexibility in the grid of a local Swiss DSO, AMB. We restricted the study to two flexible devices, Heat Pumps (HPs), and Electric Heaters (EHs). We simulated the following heating system configurations:

- HP: in this configuration, both space heating and domestic hot water (DHW) are provided by the HP. The heating system is modeled using the STASH 6 standard, which describes the most common heating configuration in Switzerland. A detailed mathematical description of the building thermal model, stratified water tanks, HP and heating system model is provided in the annex C.
- EH: in this case, the EH is just used to provide DHW, while the space heating is not modeled, the latter being considered to be fueled by gas or oil (which is still common in Switzerland).

### 2.1.1 Metadata retrieval

To faithfully simulate the flexibility potential of a region when HPs and EHs are connected to a ripple-control system, for each building we need to estimate the presence of an HP or EH, the number of dwellers (influencing DHW consumption) and the equivalent thermal resistance $R$ $[\mathrm{K\,W^{-1}}]$ and capacity $C$ $[\mathrm{kWh/K}]$ of the building. Since we can't retrieve this information without incurring in privacy issues, we instead cross-referenced available statistical information for Ticino's residential buildings:

1. We retrieve the percentage of buildings equipped with an HP or an EH in a given region using data from [13], based on the Federal Statistical Office's 2014 Buildings and Dwellings Statistics [14]. This dataset is divided into squares with a side of 90 meters. This information must be cross-referenced with the Federal Register of Buildings and Dwellings (RBD) always from [13] to retrieve the total number of HPs in a given region. An incomplete summary of this information is shown in figure 1.
2. To estimate which particular building is equipped with an HP, we used information on the building's scope of use and year of construction class in RBD's catalog of buildings. We then use statistics on the probability for single and multi-family house buildings to have an HP or an Electric heating system, from [15] and reported in figure 2. Once we have estimated the probability of a given building having an HP, we randomly assign HPs within a 90x90 meters area until the expected total number of buildings with an HP in the area is met. The same process is used to assign EHs.
3. We then combine this information with the following, summarized in figure 3:
   - the average number of $\mathrm{m}^2$ per person for buildings of a given construction age, from the Swiss Federal Statistical Office [14], which allows us to have an estimate of the number of dwellers. This information is then used to retrieve a water consumption profile and to size the heating source and buffer volume for the DHW.
   - the total annual consumption per square meter and construction age of buildings in Ticino, from [16], and the heating reference surface (HRS) from RBD, which are then used to estimate the equivalent building's thermal resistance $R$, as explained later.

A summary of the final set of parameters, the conditioning factors, and the sources used to retrieve them is reported in table 2.

| parameter | conditional on | sources |
|---|---|---|
| $R$ [K W$^{-1}$] | construction period, location, class of building | [13, 16] |
| $C$ [kWh/K] | - | [17] |
| Prob(HP EH) | construction period, location, class of building | [13, 15] |
| occupants | construction period, location, class of building | [13, 14] |

Table 2: Simulation parameters and their sources

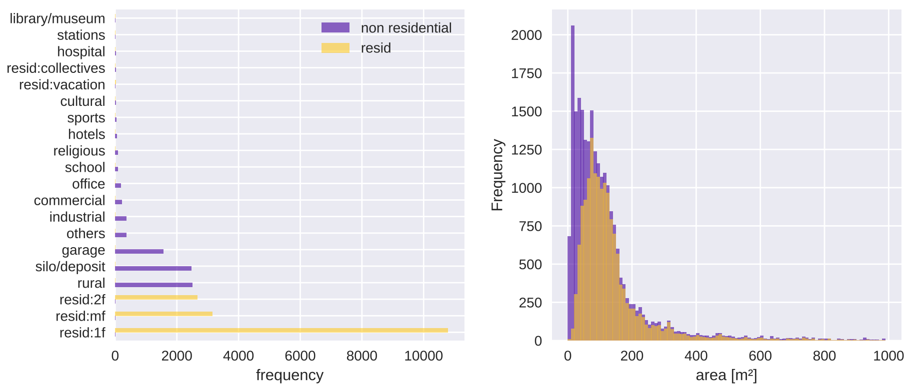


Figure 1: Statistics from RBD. Left: frequency of destination of use among the building in the AMB districts. Right: distributions of squared meters per building, conditional on being residential or not.

### 2.1.2 Component sizing

The final simulated devices have been sized starting from the available metadata as described in the following. For the region of interest, we identified around 3000 buildings having either an installed HP or an EH and a total installed nominal power of 12.5 MW and 7.7 MW for the two classes of devices. These numbers are in line with the figures that the DSO provided us with. The final distributions over the whole set of considered buildings, for some of the key metadata and device parameters, are shown in figure 4.

**Building thermal resistance** The building's equivalent thermal resistance could be assessed starting from the total building yearly consumption, which we previously estimated for each building from [16, 13]. Considering the following equation for a one-state RC thermal equivalent circuit:

$$\frac{\partial T}{dt} = R^{-1}(T_{ext} - T) + kI + Q_{int} \tag{1}$$

where $T_{ext}$ is the external temperature, $I$ is the global horizontal irradiance, $Q_{int}$ are internal heat gains and $k$ a coefficient. Assuming stationarity, we could retrieve an estimated thermal resistance averaging over one year:

$$R^{-1} = \frac{k\overline{I} + E_y}{\overline{\Delta T}} \tag{2}$$

where the average quantities for irradiance $I$ and temperature difference are obtained by integrating over the data of the simulated year, and $E_y$ is the total yearly heating consumption from [16] times the heating reference surface, expressed in kWh. In our case, however, the stationarity assumption is not a good one, since we assumed changing setpoints for the internal temperature of the buildings depending on the hour of the day, as is common practice. This makes the internal temperature subject to variations during the day, which results in (2) being a poor approximation for $R^{-1}$. To better approximate it, we simulated one year of operations for each building using a simple surrogate model and optimized

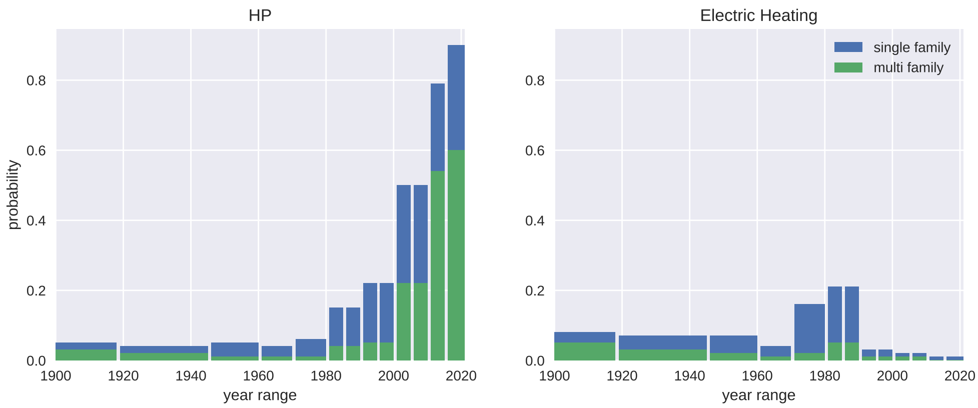


Figure 2: Probability for a building to have an HP and EH installed, conditional to the class of construction year and building destination of use.

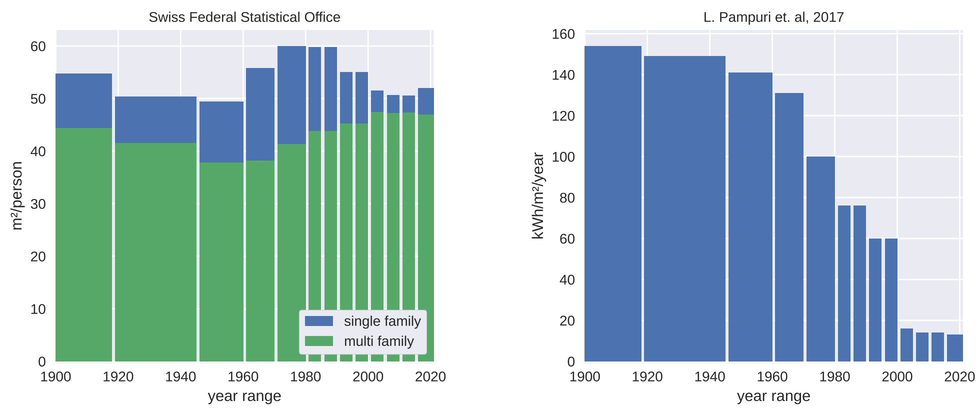


Figure 3: Representative values of m$^2$/person (Switzerland) and kWh/m$^2$/year (Switzerland, canton Ticino) for buildings, conditional to the class of construction year.

the value of $R$ via gradient descent to match the annual energy consumption $E_y$. The detailed description of this procedure is reported in annex C.4.

**Building thermal capacity** While it was possible to estimate the total equivalent resistance by cross-referencing different sources, we didn't find any statistical source for the characterization of the building's equivalent thermal capacity. As for the thermal resistance, when using an RC equivalent system to simulate the thermal dynamics of a building, the C factor is usually either estimated from temporal data or in a white box fashion, starting from buildings' stratigraphies. However, while there is a clear dependence between R and the year of construction, as shown in figure 3, due to energy-saving policies, there is no such trend for the thermal capacity. For this reason, we chose equivalent capacity factors uniformly sampling from a uniform distribution with a mean value of 2.5 MJ/m$^2$/K and cutoff values of 1 and 5 MJ/m$^2$/K, as these are the reference values indicated in the Swiss Society of Engineers and architects (SIA) norm 380/1 [17] for lightweight and high inertia buildings.

**EH sizing** The nominal power for the EH is chosen using the following formula:

$$q_{EH} = q_{DHW} = r_v n_o \tag{3}$$

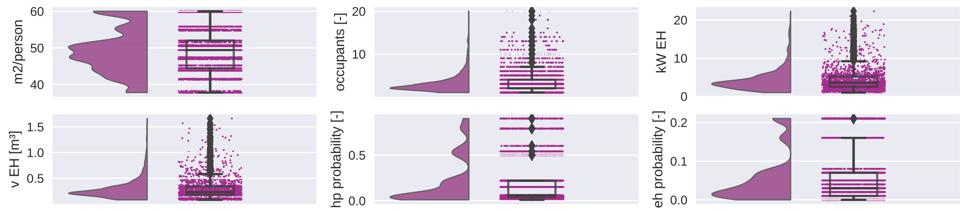


Figure 4: Final distributions of some key parameters for the simulation for the 3000 considered households

| power [kWh/person] | | volume [m$^3$/person] | |
|---|---|---|---|
| lower bound | upper bound | lower bound | upper bound |
| 1 | 2 | 0.08 | 0.12 |

Table 3: Upper and lower bounds for the uniform distribution for the sizing of the EH

where $r_v$ is a random variable drawn from the uniform distribution with limits reported in table 3, representing the kWh per person needed for heating the DHW. The variable $n_o = A/a(p,d)$ is the estimated number of occupants, derived from the total building area $A$, where $a(p,d)$ is the specific area per person and destination of use, $p$ and $d$ respectively, from [14] (depicted left in figure 3). The volume of the water tank is modeled similarly with the uniform distribution limits reported in 3.

**HP sizing** For HP sizing, we have assumed -4 and 20 $C$ as outdoor and indoor reference temperatures, respectively. The final nominal power for the HP is then chosen using the following formula:

$$q_{HP} = \text{maximum}\left(R^{-1}\Delta T_{ref} + q_{DHW}, 2\right) \tag{4}$$

where $R$ is the previously determined equivalent thermal resistance, $\Delta T_{ref}$ is 24 and $q_{DHW}$ is the nominal power for the domestic hot water. As previously stated, in this case, the HP is also the heating source for the DHW, which is sized as per equation (3).

#### 2.1.3 building thermal model validation

The thermal model of the building, whose parameters have been selected with the procedure explained in section 2.1.2, has been validated by means of annual energy consumption. The results are reported in figure 5. It can be seen how the simulated consumption is always slightly higher than the expected one (which is the annual consumption for heating from [16] multiplied by the building's total area). This is due to the fact that the optimization procedure to tune the $R$ parameter does not include thermal losses from the heating system, and the heating system logic of the surrogate model is more reactive than the one implemented in the full simulation model, where the heating is due to serpentine. The mean relative error on the yearly energy consumption is about 5% while 90% of the simulated buildings have a discrepancy lower than 9%.

### 2.2 Energy oracle for flexibility modeling and optimization

#### 2.2.1 Problem statement and methodology

We are interested in learning the aggregated power response of a group of HPs and EHs, conditional to the number of devices and a control signal, from simulations. The scope is twofold: characteriz-

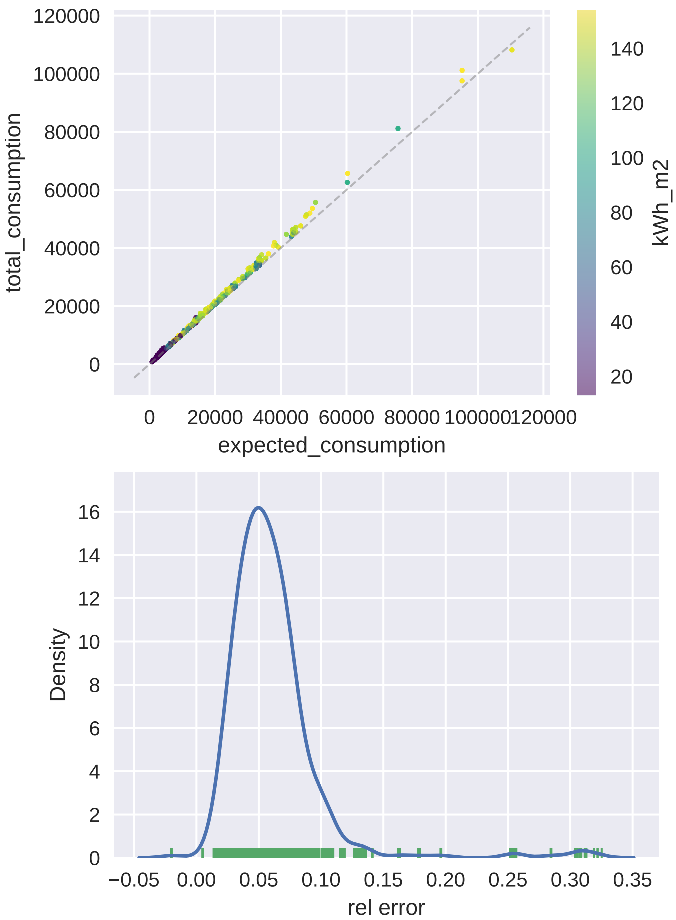


Figure 5: Validation of thermodynamic simulations by means of comparison of annual heating energy consumption for 800 randomly sampled buildings. Top: scatter plot between expected and simulated consumption. Bottom: kernel density estimation of relative error.

ing the flexibility potential beyond simulated conditions and using the learned response to optimally craft the force-off control signal. Called $x_t \in \mathbb{R}^{n_f}$ a set of $n_f$ features for a given simulated operational condition and a given group of devices, $y_t^f \in \mathbb{R}^H$ their aggregated power profile for the next $H$ steps ahead, we can define a dataset of features and targets, $\mathcal{D} = (x_t, y_t^f)_{t=1}^N$. The energy oracle $f(x, \theta) : x_t \rightarrow \hat{y}_t^f$ forecasts the power consumption of a group of flexible devices starting from the features contained in $x_t$. Since we want to retrieve a prediction conditional to the control action, $x_t$ also contains information on past and future values of the control signal $s$, which is applied to the devices. In order to learn the system response conditional to the value of the control, one could think to craft a dataset with tuples of simulations differing only in one of them having a zero control signal, all the other conditions being the same. However, it is difficult to build such a dataset, as the energy consumption of the controlled devices is also influenced by the past values of the control signal, and eliminating this dependence could require simulating several days for each pair of rows of the final dataset $\mathcal{D}$. Instead of building a dataset of controlled and uncontrolled tuples, we just simulated a controlled year and an uncontrolled one, leaving to the oracle $f(x_t, \theta)$ the task of modeling the causal relation between the control signal $s$ and the system response.

### 2.2.2 Dataset generation

In our case, $s$ is a binary signal encoding the force-off of the ripple control. This signal is not allowed to change randomly through the day but must respect some conditions, such as a minimum time in which the state must be kept fixed and a maximum number of daily activations. The simulated force-off signal has been obtained by generating all feasible force-off signals compatible with conditions reported in table 4. In figure 6, we can see a sample of the resulting force-off signals, the ratio of scenarios in which the force-off is active as a function of time-step, and the distribution of the total steps in which the force-off signal is on. It is not possible to generate all the possible combinations of binary signals and then filter them for conditions in 4, since using a 15-minute time-step will require generating ex-ante $2^{96}$ signals. For this reason, we used a dynamic programming approach, filtering out incompatible scenarios on the run, as they are sequentially generated. We report in table 4 the criteria used to craft the evaluated scenarios.

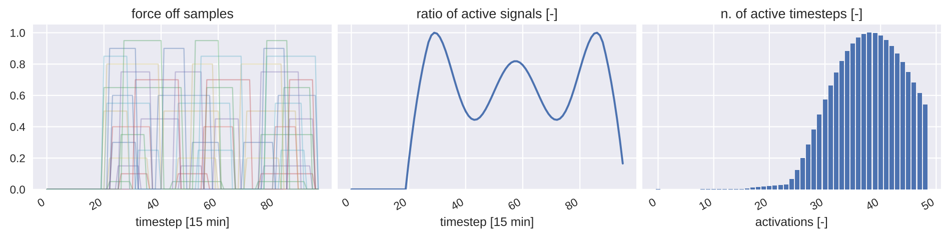


Figure 6: Left: a random sample of daily scenarios for the force-off signal. Center: ratio of active signals for a given time-step of the day. Left: distribution of number of active time-steps among all possible scenarios.

| parameter | value | description |
|---|---|---|
| tariff length | 96 | length of the force off signal |
| min segment length | 8 (2H) | min constant period |
| max changes | 6 | max number of switches in the force |
| max high | 24 (6H) | max steps when force off is on |
| off period | 20 (5H) | nightly uncontrolled period |

Table 4: Parameters used to generate all possible daily force-off signals

One purpose of the oracle is to be able to predict the response of buildings in different portions of the distribution grid. Instead of training several oracles based on the number of buildings equipped with an HP or an EH, we follow suggestions from forecasting literature, where global models are effectively trained to predict time series coming from different sources. Following this approach, we introduce penetration scenarios in the training dataset using the following procedure:

1. Run two full-year simulations for the whole set of modeled buildings; the first year is subject to the daily force-off scenarios sampled at random out of the possible ones, while the second year is simulated without controlling the devices.
2. Build penetration scenarios, grouping a subset of the simulated buildings, from which the aggregated power, $y_t^f$ is retrieved. For each penetration scenario, a dataset is then built, picking at random $k\%$ observations from the simulated years. We sampled a total of 100 penetration scenarios and used $k = 20$, for a total length of the dataset of 40 equivalent years.
3. Retrieve metadata describing the pool of buildings for each penetration scenario. Metadata includes the total number of each kind of device, the mean thermal equivalent transmittance (U) of

| penetration scenario features | temporal features |
|---|---|
| p_nom_tot, p_q_10, p_q_90, n_hp, n_eh, device_ratio, U_mean, U_q_10, U_q_90, C_mean, C_q_10, C_q_90 | hour, day of week, minuteofday |

Table 5: Metadata used as features in the training set. Penetration scenario features describe the characteristics of the pool of simulated buildings and devices, while temporal features refer to the time of the prediction.

| signals | transformation | lags |
|---|---|---|
| force off | mean(15m) | -2,-1 , 1..96 |
| | mean(1h) | -12..-1 |
| $p_t^f$ , meteo | mean(15m) | -4,..-1 |
| | mean(1h) | -168..-144, -24...-1 |
| meteo | mean(1h) | 1..24 |

Table 6: Continuous variables, transformations and lags passed as features to the oracle. Meteorological information consists of temperature and global horizontal irradiance measurements.

the sampled buildings, and other parameters reported in table 5. We further augment the dataset with time features such as the hour, the day of the week, and the minute of the day of the prediction time.

4. Augment each penetration scenario dataset through transformations and lags of the original features, as reported in table 6, to obtain $\mathcal{D}_s$.

5. Retrieve the final dataset by stacking the penetration scenario datasets $\mathcal{D} = [\mathcal{D}_s]_{1:n_s}$

#### 2.2.3 Model description

The energy oracle is a collection of multiple-input single-output (MISO) models, each of which is a LightGBM regressor [18] predicting $p_t^f$ at a different step-ahead. The alternative to a collection of MISO models is training just one MISO model after augmentation of the dataset with a categorical variable indicating the step ahead being predicted. This option was discarded due to both memory and computational time restrictions. For our dataset, this strategy requires more than 30 GB of RAM. Furthermore, the training of a single tree for the whole dataset requires more computational time than training a set of MISO predictors in parallel (on a dataset that is 96 times smaller).

We recall that the final dataset is composed of 100 scenarios differing in the set of buildings composing the aggregated response to be predicted. This means that removing observations at random when performing a train-test split would give the oracle the possibility to see the same meteorological conditions present in the training set. To overcome this, the training set was formed by removing the last 20% of the yearly observations from each penetration scenario dataset $\mathcal{D}_s$. That is, the training-test split is done such that the training set contains only observations relative to the first 292 days of the yearly simulation.

A hyper-parameter optimization is then run on a three-fold cross-validation over the training set; this means that each fold of the hyper-parameter optimization contains roughly 53% of $\mathcal{D}$. The tuned hyper-parameters are just the learning rate and the number of estimators for the LightGBM regressors; the parameters are kept fixed for all 96 models predicting the various step-ahead. We used a fixed-budget strategy with 40 samples, using the `optuna` python package [19] implementation of the tree-structured Parzen estimator [20] as a sequential sampler. An example of loss landscape for the hyper-parameter optimization is shown in figure 7.

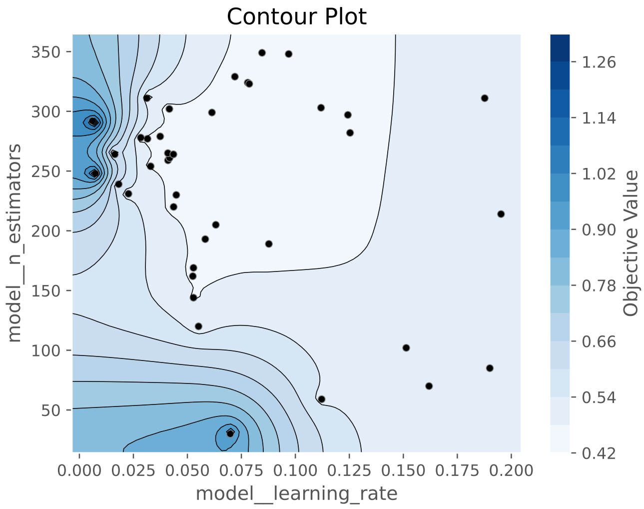


Figure 7: Loss landscape for the hyper-parameter tuning in 3 folds cross-validation for the base energy oracle with random sampling strategy.

#### 2.2.4 Ablation studies

We performed an ablation study on the model in order to see the effectiveness of different sampling strategies for the dataset formation and model variations.

**Sampling schemes** We tested two different sampling schemes for producing the penetration scenarios, described in point 2 of section 2.2.2, for the generation of the final dataset. In the first strategy, the total number of controllable devices is increased linearly, picking randomly between households with an HP or an EH. In the second strategy, the number of controllable devices is increased independently, co-varying the number of HPs and EHs, in a Cartesian fashion.

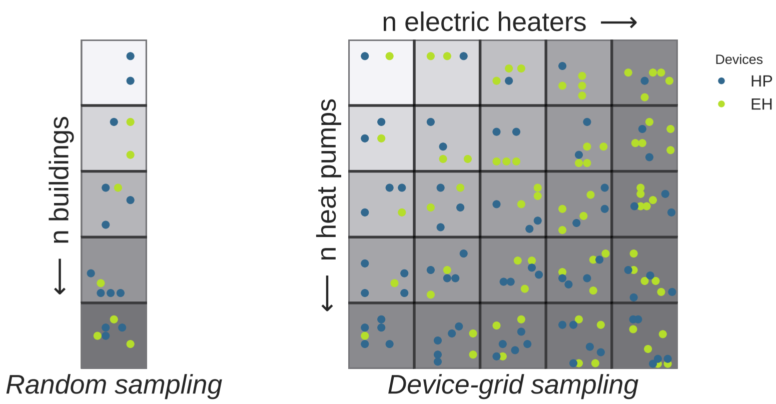


Figure 8: Sampling strategies for building the final training set. Left: the total number of controllable devices is increased linearly, picking randomly between households with an HP or an EH. Left: the number of controllable devices is increased independently, co-varying the number of HPs and EHs.

**Energy unbalance awareness** One physical insight that could help increasing the accuracy of the power oracle, is the energy unbalance. The idea is the following: we can use the oracle to predict twice the response of the system: once with the actual control signal $s$ and once with the control signals equal to $s_{ref}$ (which correspond to a zeroed force-off signal in the case of ripple control). We can then subtract the two responses to get an "energy debt" of the system for each time-step. It is reasonable to think that, under well calibrated controllers, the energy debt will balance out on a long enough prediction horizon. Even if this is not the case, having the information about the energy debt in which the system occurred at each time step could be helpful in predicting the successive ones. For this reason we tested a second model, in which at first a set of regressors predict the system response for all the steps ahead with and without the future force-off signals zeroed out. The two predictions are then subtracted to obtain the energy unbalance and this information is used to augment the training set. Finally, another set of regressor is trained on this new dataset. The same strategy is deployed at prediction time.

In total, we compared four models:

- A set of 96 independent LightGBM models, predicting the 96 steps ahead independently, trained using a random or a grid sampling in terms of HP and EH
- An energy-aware set of 96 LightGBM models, linked by the energy unbalance previously described, trained using a random or a grid sampling in terms of HP and EH

To have an idea of the oracle performances, in figure 9 we plotted 9 random examples with different numbers of controlled HPs and electric heaters out of the test set for the energy-aware oracle trained using the grid sampling strategy. In the subfigure 9a, we plotted only examples in which the force-off signal was activated at least once during the day, while in subfigure 9b we randomly selected only examples in which the devices were left uncontrolled.

To understand the dependence of the errors from different influencing factors, we plotted a heatmap of the normalized mean absolute error (MAE) as a function of the total nominal power of the of predicted samples and the step-ahead, shown in figure 10. We can see that there is a strong dependence of the oracle accuracy as a function of aggregated loads, as is expected, since aggregation has a regularization effect which helps increasing the forecastability of $p_{agg}$. The normalized MAE assumes values as low as 0.12 for the first step-ahead while increasing up to 0.28 when the nominal power is between 2 and 5 MW. No significant differences are shown among the four different models. In order to study the accuracy with respect to the prediction time, we performed a similar aggregation, shown in figure 11. It can be seen how the models are better at predicting nighttime hours, while the normalized MAE increases at peak times. Also in this case no relevant differences can be seen among the different models.

Models performances can be better compared when plotting the mean normalized MAE as a function of step ahead, as done in figure 12. The grid sampling scheme did indeed help in increasing the accuracy of the predictions w.r.t. the random sampling scheme for both the LightGBM models. Including the information about energy unbalances at each step ahead shows some benefits for both sampling strategies at the expense of a more complex overall model. The improvement in accuracy has an impact only on controlled scenarios, as demonstrated by a comparison of the second and third panels in figure 12. These panels show the scores obtained for instances where the force off signal was either activated at least once or never activated, respectively. This result aligns with our expectations. As an additional analysis, we studied the energy unbalance over the prediction horizon. For this analysis we considered just the controlled cases in the test set. We define two relative energy unbalance measures as:

$$\Delta_{rel} E_d = \frac{\sum_{t=1}^{96} \hat{y}_t(s) - \sum_{t=1}^{96} y_t}{\sum_{t=1}^{96} y_t} \tag{5}$$

$$\Delta_{rel}^{noctrl} E_d = \frac{\sum_{t=1}^{96} \hat{y}_t(s) - \sum_{t=1}^{96} \hat{y}_t(s_0)}{\sum_{t=1}^{96} y_t} \tag{6}$$

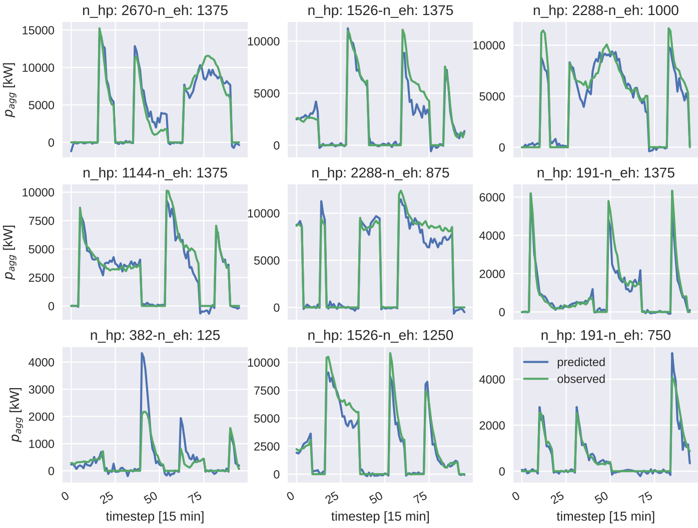


(a) Random example of day-ahead power oracle predictions for different numbers of HPs and EHs, where the force off was activated at least once.

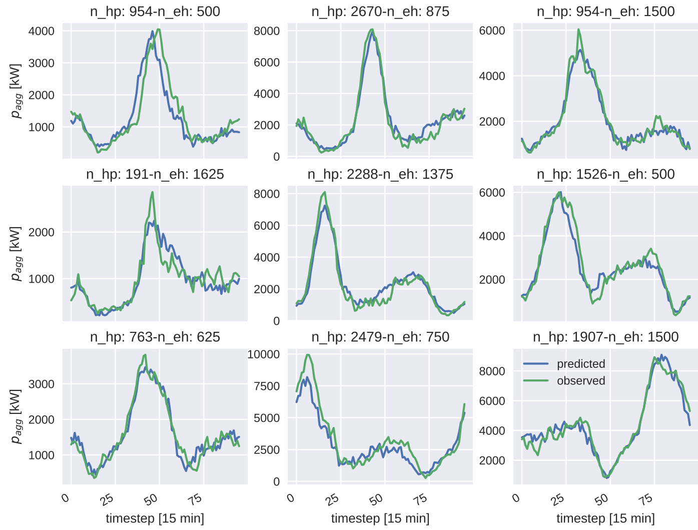


(b) Random example of day-ahead power oracle predictions for different numbers of HPs and EHs, where the force off was not active.

Figure 9: Examples of oracle predictions

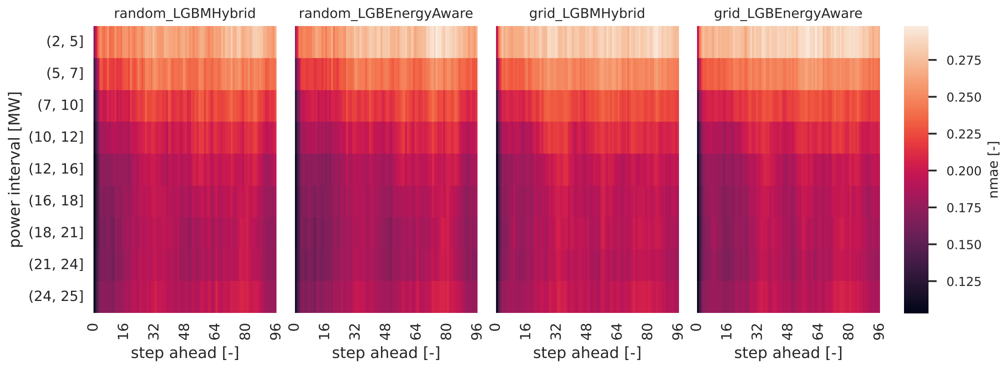


Figure 10: Normalized MAE for the four tested models for the power oracle, as a function of step-ahead and total nominal power of predicted samples.

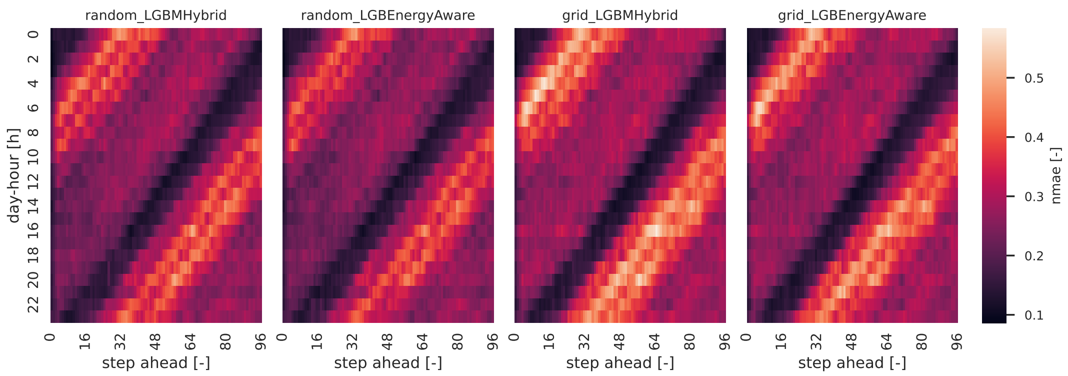


Figure 11: Normalized MAE for the four tested models for the power oracle, as a function of step-ahead and time of prediction.

where $y_t$ is the simulated power, $\hat{y}(s)$ is the power predicted by the oracle with the control used in the simulation, and $\hat{y}(s_0)$ is the power predicted by the oracle using a zero force off. We can interpret $\Delta_{rel}E_d$ and $\Delta_{rel}^{noctrl}E_d$ as the relative error in the total energy need w.r.t. the simulation and the change in the energy consumption estimated by the oracle if the pool of flexible devices were not controlled. We removed from the comparison all the instances in which the force-off signal was activated in the last 5 hours of the day. In this case, part of the consumption will be deferred outside the prediction horizon, making the comparison meaningless.

Looking at the of first row of figure 13, we see how the empirical ECDFs of $\Delta_{rel}E_d$ and its absolute value (left and right panels) are closer to zero when the model considers information on the energy unbalance. Also, applying the grid sampling strategy helps in having a more precise prediction in terms of used energy over the prediction horizon. For all 4 models, 80 % of the time the relative deviation in the horizon energy prediction lies below 20%. The second row of figure 13 reports the change in the forecast energy consumed within the prediction horizon with and without control. It is reasonable to think also in this case the consumption should approximately match, since the force off usually just defers the consumption. Also, in this case, the energy-aware models present a lower difference in the consumed energy.

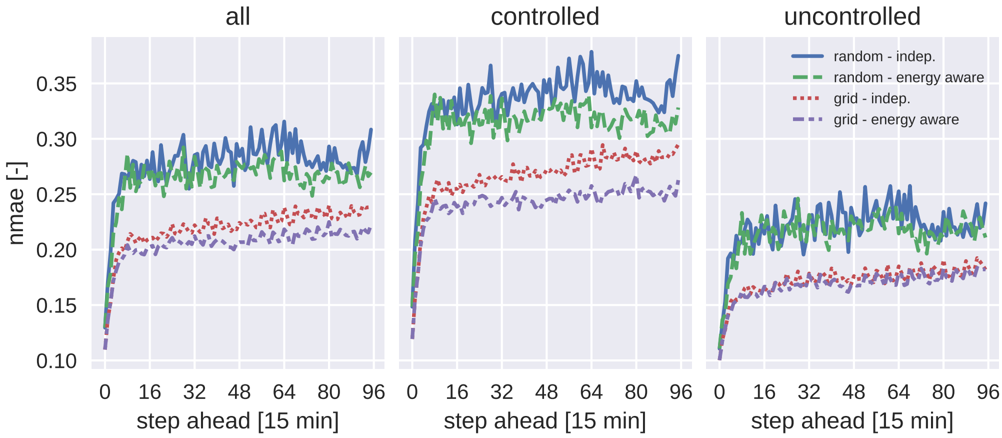


Figure 12: Performances for the four tested models for the power oracle, in terms of normalized MAE as a function of the step ahead.

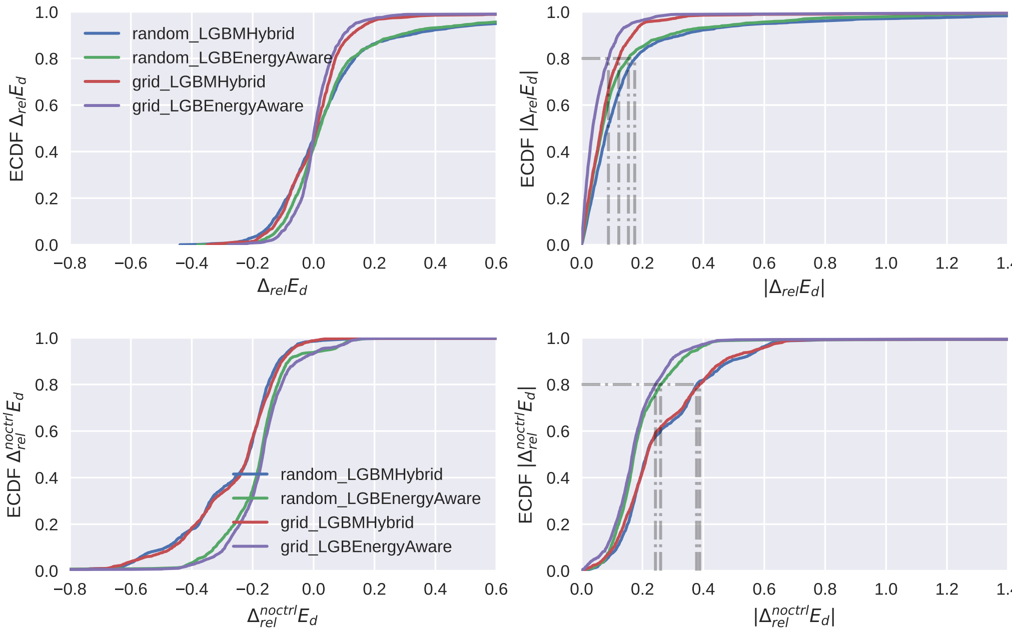


Figure 13: Left: cumulative un-normalized distribution of the relative energy unbalance error. Right: inverse cumulative function of the absolute normalized energy unbalance.

#### 2.2.5 Characterization of the rebound effect

We finally used the energy unbalance aware model in combination with the grid sampling strategy to visualize rebound effects for different numbers of HPs and EHs. Figure 14 shows three extreme examples of the characterization: the penetration scenario with the maximum number of EHs and zero HPs, the converse, and the scenario where both penetrations are at their maximum value. The rebound is shown in terms of energy unbalance from the test set, such that they have a force-off signal turning off at the fifteenth plotted step. It can be noticed how different observations can start to show a negative energy unbalance at different time steps; this is due to the fact that force-off signals can have different lengths, as shown in figure 6. The upper left quadrant show the energy unbalance predicted by the oracle in the case of maximum number of EHs and no HPs. Comparing it with the lower right quadrant, where the sample just contains HPs, we see a much smaller tau; that is, the rebound effect has a quicker decay, being close to zero after only 10 steps (corresponding to 1 and a half hour). The lower right quadrant shows a much slower decay of the rebound effect; this is due to the different heating logic and time constants of the systems heated by EHs and HPs. The EHs are used only for DHW heating, their activation is regulated by an hysteresis using two temperature sensors placed at different height of the water tank. On the contrary, the HPs are used for both DHW and space heating, and their activation is regulated by the temperature of the hydronic circuit decoupling the HP and the building heating elements (serpentine). This means that the activation of the HPs is influenced by a system with much higher heating capacity compared with the one of the DHW tank alone: the one of the building. The responses in figure 6 were colored by the seven days average of the ambient temperature. As expected, the EHs responses are not dependent on the average external temperature, while a slight effect can be seen for the HPs, where higher average temperatures correspond to faster decay of the response.

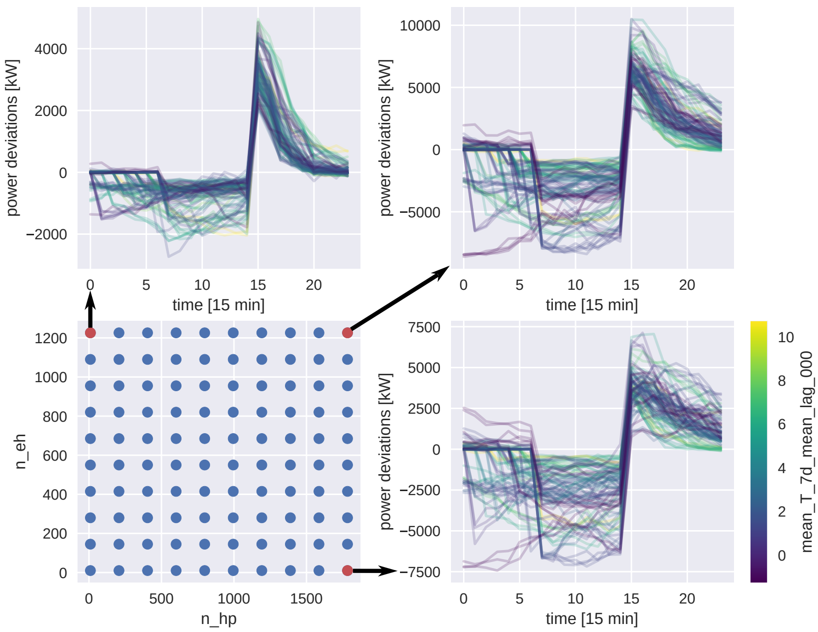


Figure 14: Example of system response in terms of deviations from expected response (prediction where control signal features referring to feature time-steps are zeroed), dependent on the number of HPs and EHs.

## 2.3 Integrating the energy oracle in the optimization loop

In this section we describe how the energy oracle can be integrated into the optimization loop, starting from the optimization of a single group of flexibility. We identified as most interesting for both the DSO and TSO perspectives, the joint minimization of the day ahead costs (paid by the DSO on the spot market) and of the peak tariff (paid by the DSO to the TSO). The latter is proportional to the monthly maximum peak over a 15 minutes interval. This cost is much more difficult to optimize with respect to the day-ahead cost since it involves solving an optimization problem over one month; over such long periods of time power forecasts cannot be accurate. As a heuristic, we solve this problem day by day: if the DSO reduces systematically its peak each day of the month, the monthly peak will be reduced. This leads to the following optimization problem:

$$s^* = \underset{s}{\text{argmin}}\, \mathcal{L}(\hat{y}(s)) \tag{7}$$

$$= \underset{s}{\text{argmin}} \left( \sum_{h=1}^{H} p^s_h \hat{y}_h(s) \right) + p^p \max_h \hat{y}_h(s) \tag{8}$$

where $h$ refers to the step ahead, $p^s \in \mathbb{R}^T$ is the day-ahead spot price and $p^p$ is the price for the monthly peak in $CHF/kW$. This is not trivial to minimize, since it's a function of a non-parametric regressor, the energy oracle. However, the parameters reported in table 4 produce a total of 62482 control scenarios; this allows us to evaluate (7) using a brute-force approach, finding the exact minimizer $s^*$. This is done through the following steps:

1. Forecast the total power of the DSO: $\hat{y}^{tot} = f_{tot}(x_t, \theta_{tot})$. An example of forecast values on the training set can be seen in figure 15.
2. Forecast the baseline consumption of flexible devices, $\hat{y}^f(s_0) = f(x_t, s_0, \theta)$, using the energy oracle with the control signal $s = s_0$ set to zero (corresponding to not controlling the devices).
3. Forecast the response of flexible devices under a given control scenario $s$ for the next day. This is always done using the energy oracle: $\hat{y}^f(s) = f(x_t, s, \theta)$.
4. The objective function is evaluated on $\hat{y}_t(s) = \hat{y}^{tot} - \hat{y}^f(s_0) + \hat{y}^f(s)$ for all the possible plausible control scenarios; the optimal control scenario $s^*$ minimizing the total costs is returned.

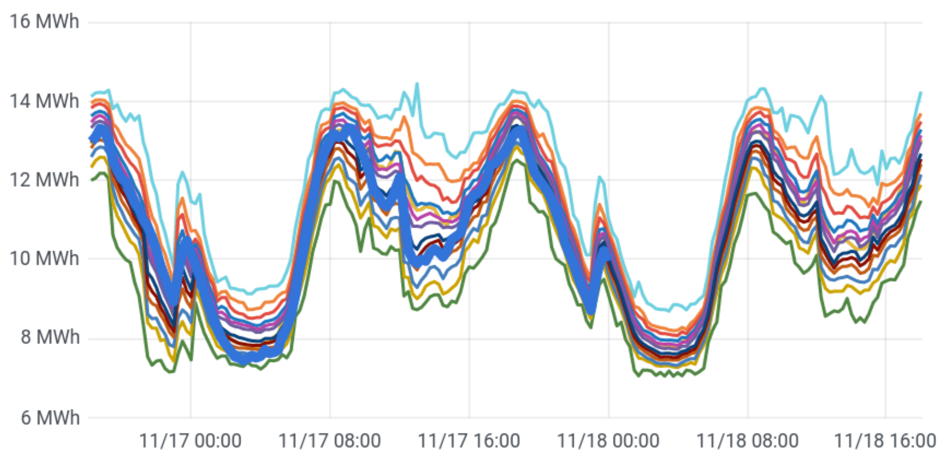


Figure 15: Example of prediction of $\hat{y}_{tot}$, obtained using the forecaster trained by Hive Power. Blue line: realized power. Thin lines: quantiles from 0.01 to 0.99.

Figure 16 shows an example of the results of the described control process. The upper panel shows the total forecasted power of AMB, $\hat{y}_{tot}$ colored in blue, the optimal proposed power profile $\hat{y}(s^*)$, and the other two scenarios with the closest costs among all the evaluated ones.

### 2.3.1 Dynamic grouping strategies

As shown in the previous section, it is convenient to divide flexible devices into more than one group. In this way comfort constraints of different users can be easier respected; secondly, it is possible to

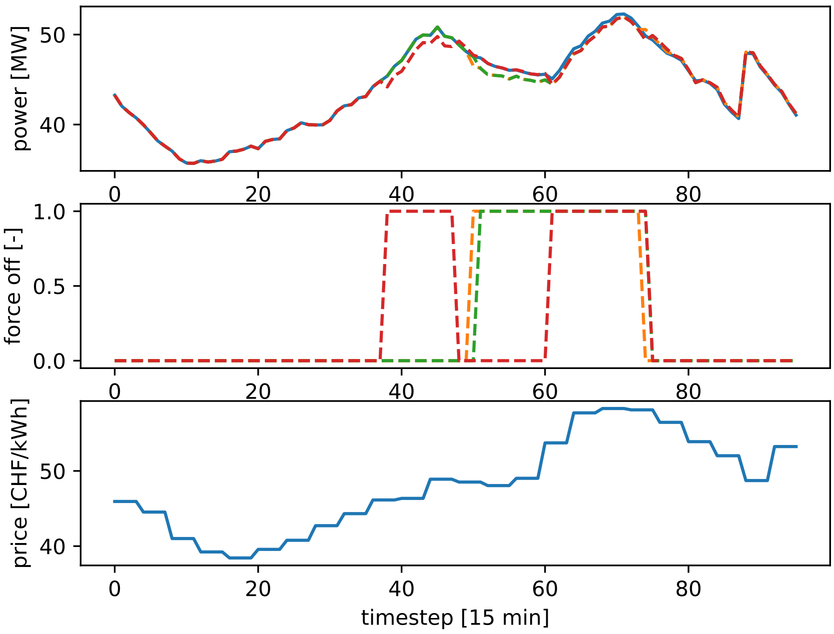


Figure 16: Example of optimized control action using the energy oracle. Top: the day ahead forecasted power profile of AMB (blue) and the three most profitable scenarios (dashed lines). Middle: the three most profitable scenarios in terms of force-off signals among the considered ones. Bottom: day-ahead price on the spot market.

exploit the flexible characteristics of different types of devices. For example, electric heaters can be turned off for longer periods of time w.r.t. HPs. Problem (7) can be reformulated as:

$$s^* = \underset{[s_g]_{g=1}^G}{\text{argmin}} \sum_{h=1}^{H} p_h^s \left( \hat{y}_h^{tot} - \sum_{g=1}^{G} \hat{y}_{h,g}^f(s_0) + \sum_{g=1}^{G} \hat{y}_{h,g}^f(s_g) \right) + \tag{9}$$

$$p^p \max_h \sum_{h=1}^{H} \left( \hat{y}_t^{tot} - \sum_{g=1}^{G} \hat{y}_{h,g}^f(s_0) + \sum_{g=1}^{G} \hat{y}_{h,g}^f(s_g) \right) \tag{10}$$

where $G$ is the total number of groups and $s_g$ is the control signal sent to the $g_{th}$ group. Problem (9) is a combinatorial problem; to reduce its complexity, we have used a sequential heuristic: the first group of devices optimizes on the uncontrolled power profile $\hat{y}_t^{tot}$. Once their optimal control for the first group is found, the second group it's optimally scheduled on $y_t^{tot} - \hat{y}_{t,1}^f(s_0) + \hat{y}_{t,1}^f(s)$, where the second subscript in $\hat{y}_{t,1}$ refers to the control group.

An example of such sequential optimization is shown in figure 18, where the scheduling of two groups of devices is shown side by side. At first, a group containing only electric heaters is scheduled, and the second group of HPs is optimized afterward. Figure 19 shows another example of sequential optimization for the same day. In this case, we used a second set of force-off scenarios for the group of electric heaters, this time allowing for longer force-off periods.

### 2.3.2 Grouping strategies for HPs

For HPs, we chose a grouping strategy based on the energy signature of the controlled buildings. In buildings heated by a thermo-electric device, such as an HP, the energy consumption is strongly (inversely) correlated with the external temperature. The energy signature refers to a linear fit between the daily energy consumption of the building and the average daily external temperature $T_d$. Since an increasing number of households have an installed PV power plant, we also include a daily average of the global horizontal irradiance $I_d$ as a feature in the energy signature fit; high values of $I_d$ could lower the daily energy consumption if a PV plant is present, but this effect cannot be imputed to the action of temperature. Without including $I_d$ in the regression, the daily energy consumption as a function of temperature could be underestimated. The final energy signature $e(T_d, I_d)$ is a piecewise linear function of the external temperature and $I_d$. An example of an estimated energy signature is shown in figure 17.

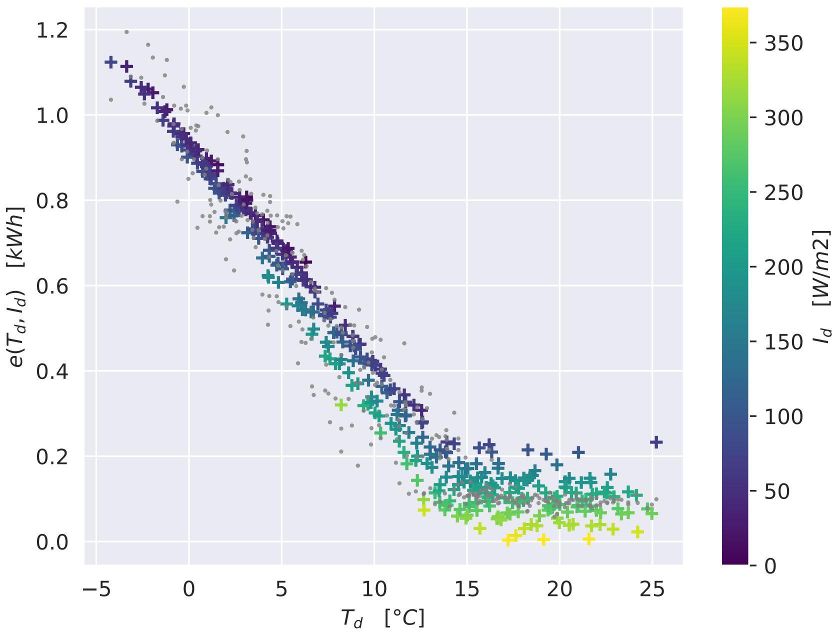


Figure 17: Energy signature example. The average daily consumption for a household is estimated with a (piece-wise) linear function of temperature and solar irradiance. Gray dots: original observations. Crosses: fit results, colored by $I_d$

Finally, to retrieve the total number of activation hours $h$, we simply divide the energy signature with the nominal power:

$$h(T_d, I_d) = \frac{e(T_d, I_d)}{p_{nom}} \tag{11}$$

The following steps describe our procedure to generate and control HPs groups based on their estimated activation time:

1. Estimate the energy signatures of all the buildings with an installed HP $e_i(T_d, I_d)$
2. Estimate their reference activation time $h_{ref,i}$ for worst-case conditions, that is, for $T_d = 0$ and $I_d = 0$.
3. Households are grouped together based on their reference activation time: $G$ control groups are defined based on linearly spaced quantiles of $h_{ref}$.
4. At control time, do a day-ahead estimation of activation times for all the HPs, $h_i(\hat{T}_d, \hat{I}_d)$ using a day-ahead forecast of $T_d$ and $I_d$. Use the within-group maximum values of the needed activation time, $h_{max,g} = \max_{i \in \mathcal{G}} h_{g,i}(\hat{T}_d, \hat{I}_d)$ to filter out control scenarios having more than $h_{max,g}$ force-off

steps. This process guarantees that all HPs are allowed on for a sufficient time, given the temperature and irradiance conditions.

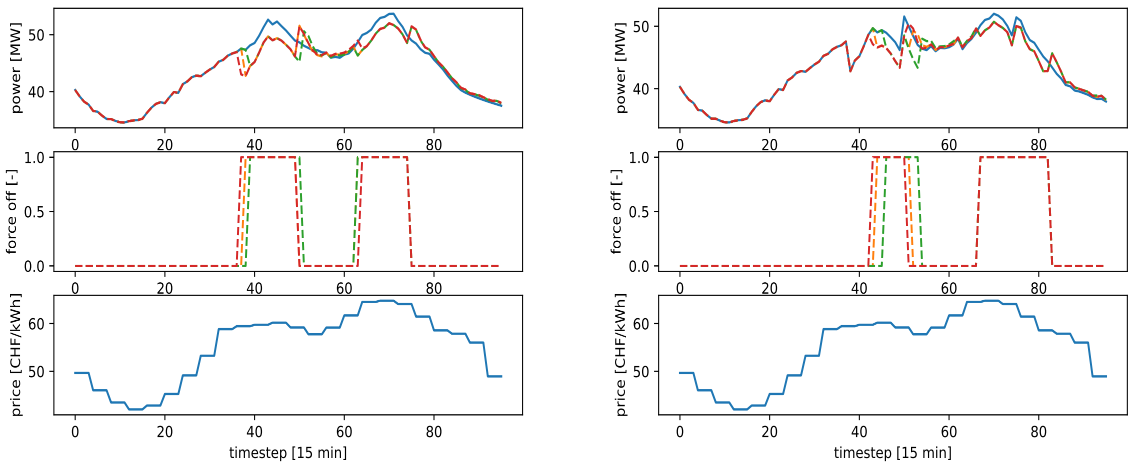


Figure 18: Example of sequential control. The first group of flexibilities (boilers) is optimally scheduled (left) and the second one (HPs) is optimized considering the power profile from the first optimization (right).

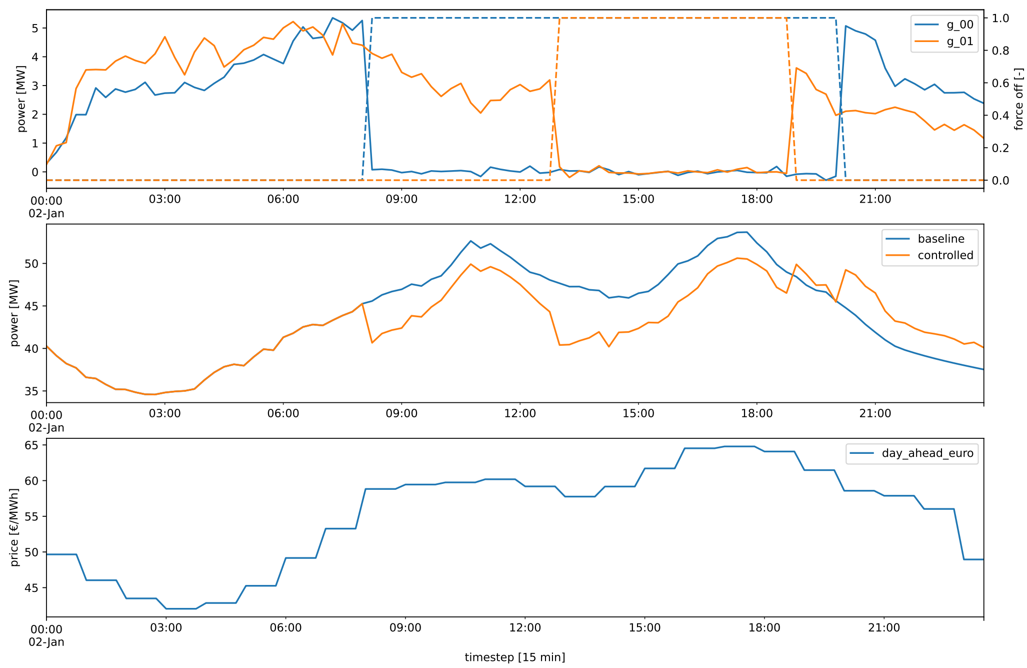


Figure 19: Another example of sequential control for the same day is shown in figure 18, but allowing the force off signal to stay on for a longer number of hours for the group of electric heaters ($g_{00}$). Top: power profiles predicted by the energy oracle for the boilers and the HPs groups. Middle: the forecasted baseline $\hat{y}_{tot}$ and the optimized profile $\hat{y}(s)$. Bottom: price profile.

## 2.4 Energy oracle operational and closed loop accuracy

For testing operational and closed-loop accuracy, we simulated 8 months of optimized operations in the grid of AMB, in the case in which 66% of the available flexibilities are controlled. We used a total of 3 control groups: 1 containing only EHs, which can be forced off for a longer period of time, and 2 groups of HPs, obtained and controlled as explained in the previous section.

The prediction error accuracy was already studied in the sections 2, where we tested the oracle on a test set of simulations. In that case, the force-off included in the dataset were random, as we couldn't already optimize them. We further tested the performance of the energy oracle when predicting the optimized force-off. The difference is that the actual optimal force-off is more correlated than the random ones observed during training, and the performance could be different. Besides this, we also assessed the accuracy of the oracle in terms of economic results, in closed-loop; that is, we retrieve the errors on the economic KPIs when the simulation is completely bypassed and the oracle is used for both optimizing and emulating the behaviour of the controlled devices.

**Open loop operational accuracy** At first, operational accuracy was assessed in terms of predictions, comparing the aggregated controlled power profile with sum of the individually simulated (controlled) devices. Figure 20 shows the normalized daily time series of the prediction error during the actual optimization process. This is defined as:

$$n\epsilon_d = \frac{y_d - \hat{y}_d}{y_d} \tag{12}$$

where $y_d, \hat{y}_d \in \mathbb{R}^{96}$ are the aggregated simulated power profiles and their day ahead predictions, respectively.

We see that for all the observed error paths we just have sporadic deviations above 10%. To have a more general understanding of the oracle performance, in the second panel of 20 we plotted the histogram of the mean daily error, defined as $\frac{1}{96}\sum_{i=1}^{96} nE_{d,i}$. This shows that the energy oracle is usually under-predicting, or over-smoothing, the true response from the simulation, which is in general the expected behaviour of a forecaster trained minimizing the sum of squares loss. The fact that this distribution is contained in the -2%-3% interval, which is much narrower than in the maximum observed discrepancies in the daily error traces, confirms that high error deviations in the day ahead predictions are just sporadic.

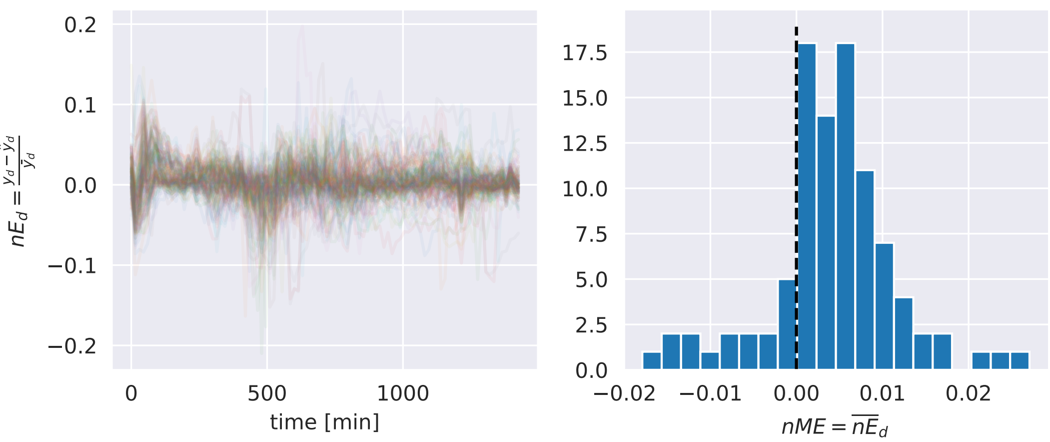


Figure 20: Performance of the oracle in the open-loop simulations. Left: daily relative errors plotted as time series. Right: distribution of the daily means of the relative error.

**Closed loop economic performances** We cannot directly assess the closed-loop performances of the oracle in terms of prediction errors. This is due to the fact that, when simulating in closed-loop, the predictions of the oracle are then fed to itself in a recurrent fashion. This could result in slightly different starting conditions for each day; furthermore, the comparison of the sampled paths is not our final goal. A more significant comparison is in terms of economic returns. We compared these approaches:

1. Simulation: we run the optimization and fully simulate the system's response. In this setting, the oracle is just used to obtain the optimal control signal to be applied day ahead. The controlled devices are then simulated, subject to the optimal control signal. The costs are then computed based on the simulations.
2. Forecast: for each day, the optimal predictions used for the optimization are used to estimate the cost. We anyways simulate the controlled devices; this process is repeated the next day. This approach gives us an understanding of how the operational prediction errors shown in figure 20 impact on the estimation of the costs.
3. Closed-loop oracle: the simulations are completely bypassed. The oracle is used for both optimizing the control signal and generating the next-day responses for the controlled devices.

It should be clear that, if the third approach gives comparable results in terms of costs, we could then just use the energy oracle for both the control task and its evaluation. This would significantly speed up the simulation loop: we won't have to simulate the thermodynamic behavior of thousands of households, but just evaluate the trained oracle, which evaluation is almost instantaneous. This could seem unlikely to reach the same accuracy produced by a detailed simulation, but this can be justified by the fact that we're only interested in an aggregated power profile, whose dimensionality is just a tiny fraction of all the simulated signals needed to produce it.

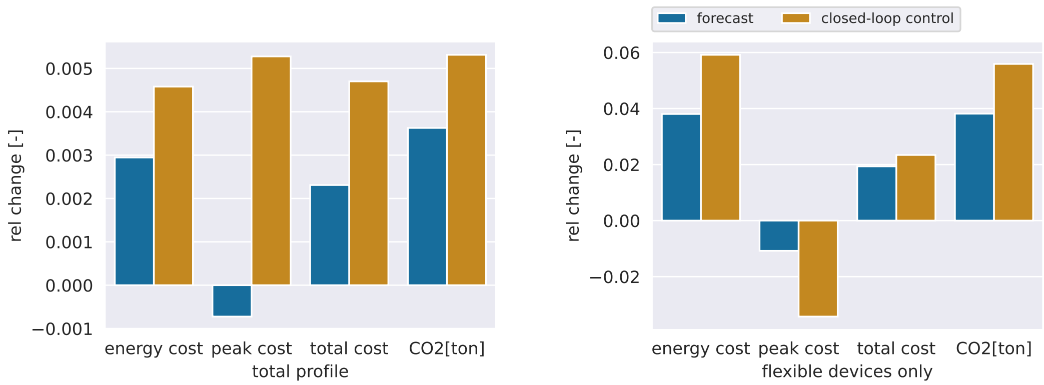


Figure 21: Deviations of different objectives from the simulated results, using the energy oracle to optimize and forecast the power profiles (blue) or to completely bypass the simulation (orange). Left: objectives computed on the aggregated profile $y$. Right: objectives computed on total power of flexible households only, $y^f$.

In figure 21, we reported the relative discrepancies from economic KPIs retrieved by the simulation using the two aforementioned approaches. As an additional KPI, we also reported the estimated tons of produced $CO_2$. While the $CO_2$ emissions are not directly optimized for, minimizing the energy costs also have a positive impact on the emissions, since energy prices correlate with the $CO_2$ intensity in the energy mix. The emitted $CO_2$ tons are estimated as:

$$M_{C0_2} = \sum_{t=1}^{T} C_t y_t \tag{13}$$

where $C_t$ is the carbon intensity in the national energy mix in $\frac{g_{CO_2}}{kWh}$. The right panel refers to the costs that would generate just considering the aggregated power profile of flexible households, $y^f$. In our case study, the controlled group of devices is just a small fraction of the total energy delivered by the DSO; to estimate the oracle's performance it's thus important to evaluate only costs generated by controlled devices. The blue columns show the relative deviations of the KPIs computed using the energy oracle's forecasts: for both the energy costs and the $CO_2$ we have a relative error below the 4% w.r.t. the value obtained by the simulation. For the closed-loop case, corresponding to the orange columns, we have a higher deviation but limited to 6%. These discrepancies can still be considered reasonable to perform A/B testing in simulation.

| | simulated | rel. diff. forecasts | rel.diff. closed loop |
|---|---|---|---|
| Energy cost | 1.27E+7 | 2.95E-3 | 4.58E-3 |
| Peak cost | 2.68E+6 | -7.23E-4 | 5.28E-3 |
| Total cost | 1.54E+7 | 2.31E-3 | 4.7E-3 |
| $CO_2$[ton] | 32816.9 | 3.63E-3 | 5.31E-3 |

Table 7: First column: costs of energy, peak, total costs and $CO_2$ emissions from the controlled simulation. Second column: relative differences from the simulated costs when they are evaluated using the day-ahead predictions from the oracle. Third column: relative differences from the simulated costs using the oracle to emulate the system. Data refers to the case in which 66% of the available HPs and boilers were controlled.

| | simulated | rel. diff. forecasts | rel.diff. closed loop |
|---|---|---|---|
| Energy cost | 9.62E+5 | 3.81E-2 | 5.91E-2 |
| Peak cost | 6.00E+5 | -1.07E-2 | 3.42E-2 |
| Total cost | 1.56E+6 | 1.93E-2 | 2.34E-2 |
| $CO_2$[ton] | 3058.2 | 3.82E-2 | 5.59E-2 |

Table 8: First column: costs of energy, peak, total costs and $CO_2$ emissions from the controlled simulation, considering only simulated devices. Second and third columns as for table 7

The left panel shows discrepancies for actual costs faced by the DSO, computed using the total power profile $y$. In this case, we have roughly a ten-fold reduction in the relative error w.r.t. the simulations. This is not a surprise, since as anticipated, the controllable devices constitute only a fraction in terms of energy supplied by the DSO. Nevertheless, this is the quantity we are interested in. For completeness, the relative deviations and absolute costs for the simulated case relative to figure 21 are reported in tables 7 and 8 for the total and flexible device profiles, respectively.

## 2.5 Impact of dynamic tariffs in the activation of flexibility

In this section, we consider the possibility of modeling and including the effect of indirect control, i.e. a dynamic energy tariff, on the aggregated power profile. We expect in general such an effect to be smaller than the one achievable by direct control; the research question we tried to answer is whether or not the measured effect was statistically significant and keen to be modeled using a data-driven approach. AMB offers a dynamic tariff to its clients since 2021 and 350 users opted in as March 2022. The dynamic tariff is a bi-level tariff, communicated a day ahead to the clients. The purpose of the tariff is to try to steer the demand away from the hours of peak demand; that is, based on the forecast aggregated power profile of AMB, the periods of high prices are placed where the daily peak demand is more likely to happen. Since all the users see the same tariff, users' power and the tariff can be treated as being statistically independent. We analyzed the data from the group of users who opted-in to the dynamic tariff in the period going from March 2021 to March 2022. In order to see any effect induced by the dynamic tariff, we defined a control group. This is composed by 1500 residential meters with similar power consumption from the municipality of Claro. A comparison in terms of profiles and quantiles of the time series of the two groups can be seen in figure 22. Since some households from Claro signed in for the dynamic tariff, they were removed from the control group.

We applied a basic variant of regression discontinuity [21], to see if being in the dynamic tariff influences the consumption of the end users. Briefly speaking, we compared the average consumption of the end users between periods of high and low tariffs. If the dynamic tariff has the intended effect, that is, shifting consumption from periods of high tariffs to periods of low tariffs, we should see a lower power consumption during periods of high tariff from users who adopted the dynamic tariff when comparing them with the control group. Figure 23 shows an example of the computation of the mean consumption under high and low tariff periods for a single user in a random day. Formally, we compared two groups in terms of the following quantity:

$$\Delta p_u = \frac{1}{n_{low}} \sum_{t \in \mathcal{T}_{low}} p_{u,t} - \frac{1}{n_{high}} \sum_{t \in \mathcal{T}_{high}} p_{u,t} \tag{14}$$

where $u$ stands for the $u_{th}$ user, $\mathcal{T}_{low}$ and $\mathcal{T}_{high}$ stand for the set of times in which the tariff is low and high, respectively, and $n_{low}$ and $n_{high}$ are the cardinalities of the two sets. Called $\mathcal{D}$ and $\mathcal{C}$ the groups of users who adopted the dynamic tariff and the control group, the dynamic tariff has the intended effect if the difference in consumption between low and high tariff periods is higher in expectation for the users who adopted the dynamic tariff, $\mathbb{E}_{\mathcal{D}}\Delta p \geq \mathbb{E}_{\mathcal{C}}\Delta p$.

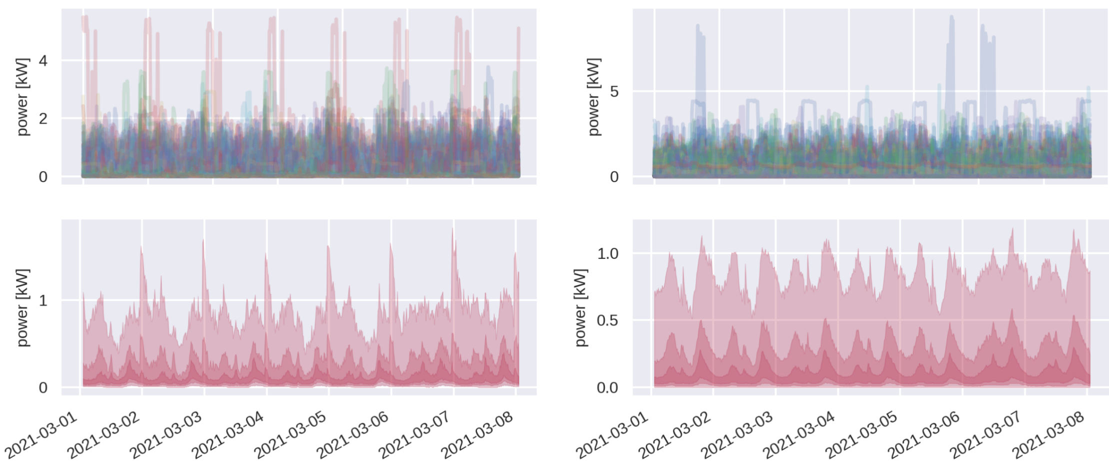


Figure 22: Left: households using the dynamic tariff. Right: households from the control group of Claro. Top: time series. Bottom: quantiles.

Figure 24 shows the distribution of $\Delta p$ for the two groups of users. We can see a slight shift towards higher values for the users in the dynamic group. The difference can be better appreciated by looking at the boxplots of the two distributions, plotted in figure 25. We can see that the mean of $\Delta p$ for the control group is below zero. This is expected since the dynamic tariff is designed to be high in periods of higher consumption. Similarly, the distribution of $\Delta p$ for the $\mathcal{D}$ group being centered on zero doesn't mean that the dynamic tariff had no effect on this group. To investigate whether the difference in the two distributions is statistically significant, we run a two-sample Kolmogorov-Smirnov test. The two distributions are different with high confidence (p-value = 1.44e-15); dynamic control group meters have higher values on average than the control group with high confidence (p-value = 8.70e-16). We can further investigate the effect of the dynamic tariff on users' consumption by plotting the two distributions as a function of the hour of the day, as done in figure 26. We can see that the two groups differ the most during daytime; at the same time, both groups show higher positive values between 11 a.m. and 18 a.m., meaning in these hours, they are more likely to consume more during low-tariff periods.

The results of the analysis show that the dynamic tariff seems to have a slight effect on the distribution

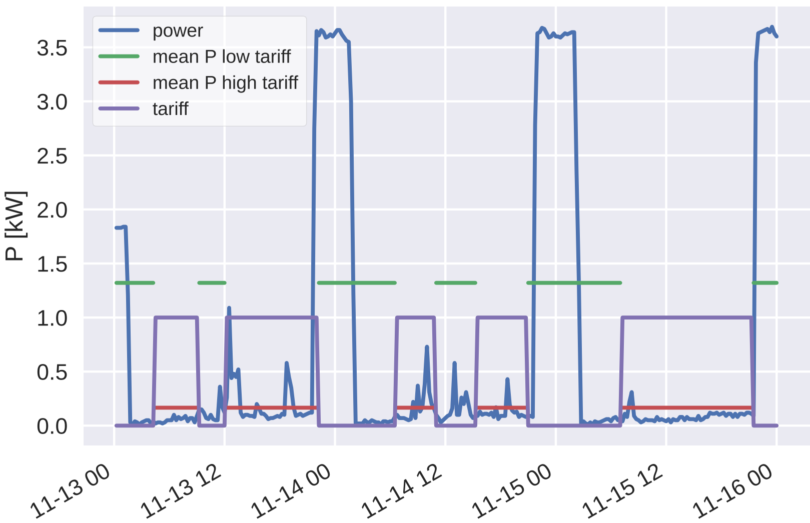


Figure 23: Example of computation of the mean average consumption in periods of high and low tariff. The green line depicts the average power for the low tariff period, while the red line represents the average power for high tariff periods.

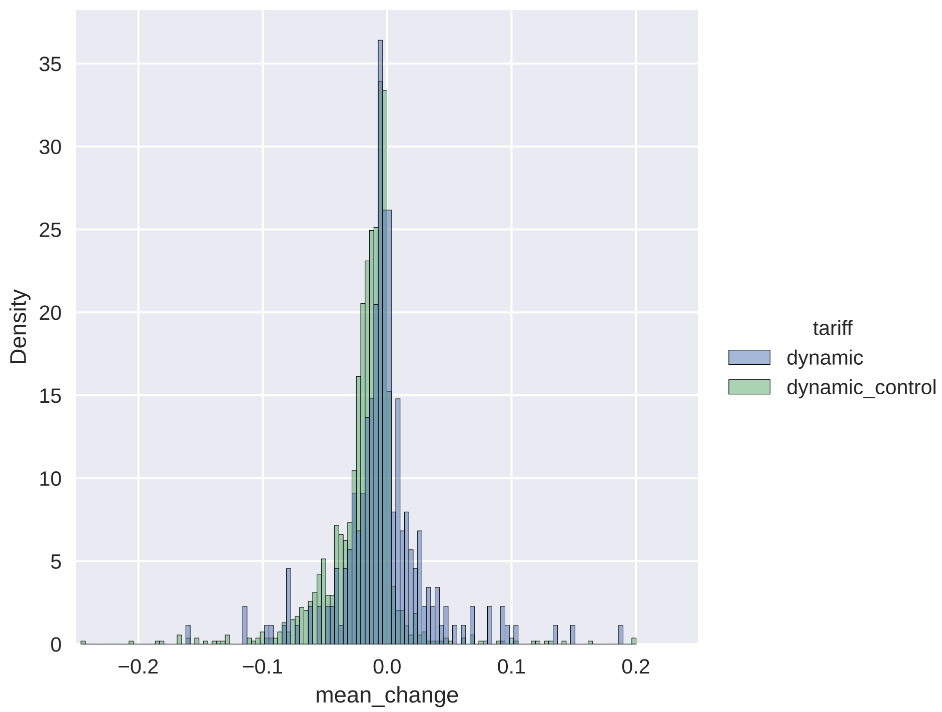


Figure 24: Distributions of $\Delta p$ for the group of users adopting the dynamic tariff (blue) and for the control group (green).

of meters' power consumption when compared with a control group. In other words, there is a statistically significant difference in the distribution of consumption, but this is not statistically meaningful; the

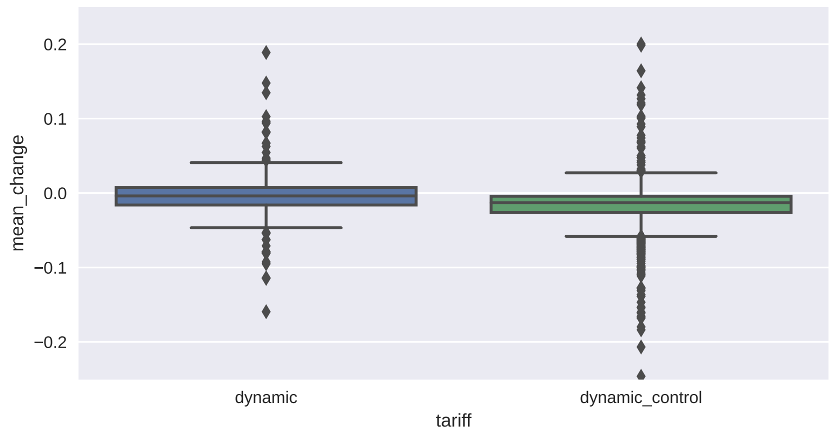


Figure 25: Boxplots of $\Delta p$ for the group of users adopting the dynamic tariff (blue) and for the control group (green).

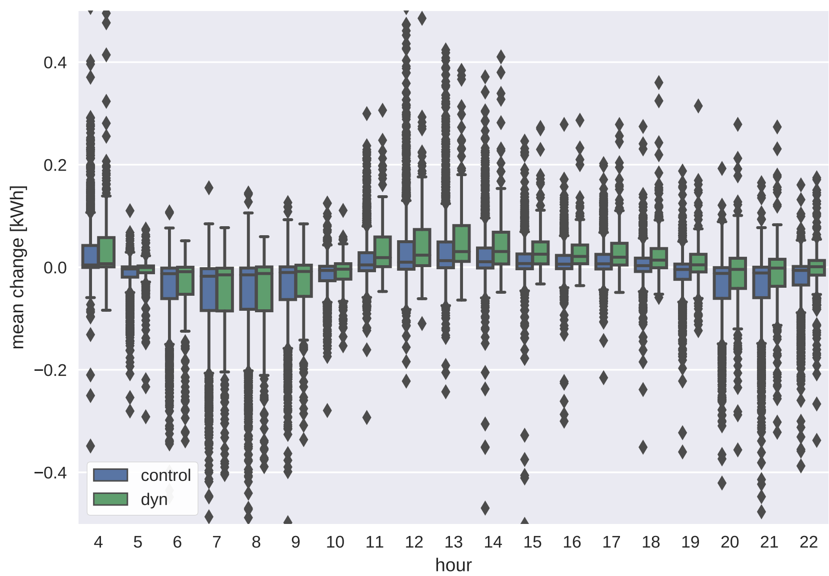


Figure 26: Boxplots of $\Delta p$ for the group of users adopting the dynamic tariff (blue) and for the control group (green), as a function of the hour of the day.

influence of the tariff on consumption is not strong enough to be modeled by a regressor more complex than the mean prediction. Furthermore, we cannot rule out a selection bias effect: since the tariff is opt-in, the users choosing the dynamic tariff could be more prone to change their consumption due to the change in the tariff. This means that the seen change in consumption could be different if the tariff is applied to all the customers of AMB. This makes it difficult to extrapolate the results in roll-out scenarios of increasing dynamic tariff acceptance. Since, as expected, the effect of indirect control is anyway much lower than the effects of direct control, we didn't include these in the scalability scenarios. However, the effect of the dynamic tariff on aggregate power consumption can surely increase by introducing smart algorithms, automatically forcing off "big" power loads as a function of the tariff.

## 2.6 Retrieval of costs for the scalability analysis

Given the energy oracle accuracy assessment summarized in figure 21, we can conclude that the energy oracle can be effectively used to approximate the simulation results in terms of total system costs. This allowed us to simulate a matrix of different penetrations, systematically changing the number of controlled HPs and EHs.

In the first step, we simulated four levels of penetration for both types of devices, resulting in 16 total yearly simulations. For all these combinations, we retrieve the energy costs, peak costs, and $CO_2$ tons. Since we obtained a regular pattern for these costs, we upsampled the results using an 11x11 grid in terms of the number of devices. The results in terms of total economic costs, as a function of controllable devices, are presented in figure 47. The matrix spans on order of magnitude in terms of avoided costs, w.r.t. the case in which no devices are controlled. The least profitable case is the one in which we just control 779 electric boilers; in this case we estimate an annual saving of 19k CHF. The most profitable case is the one in which we control all the considered devices, that is, 7790 EHs and 12517 HPs respectively. This case results in annual savings of 640 kCHF. Of this saving, only 58 kCHF comes from the optimization of peak tariff. Always referring to the maximum HPs and EHs penetration, we estimated 470 tons of avoided $CO_2$. The full matrices for the different penetration scenarios for energy costs, peak costs and avoided emissions are reported in the annex B.

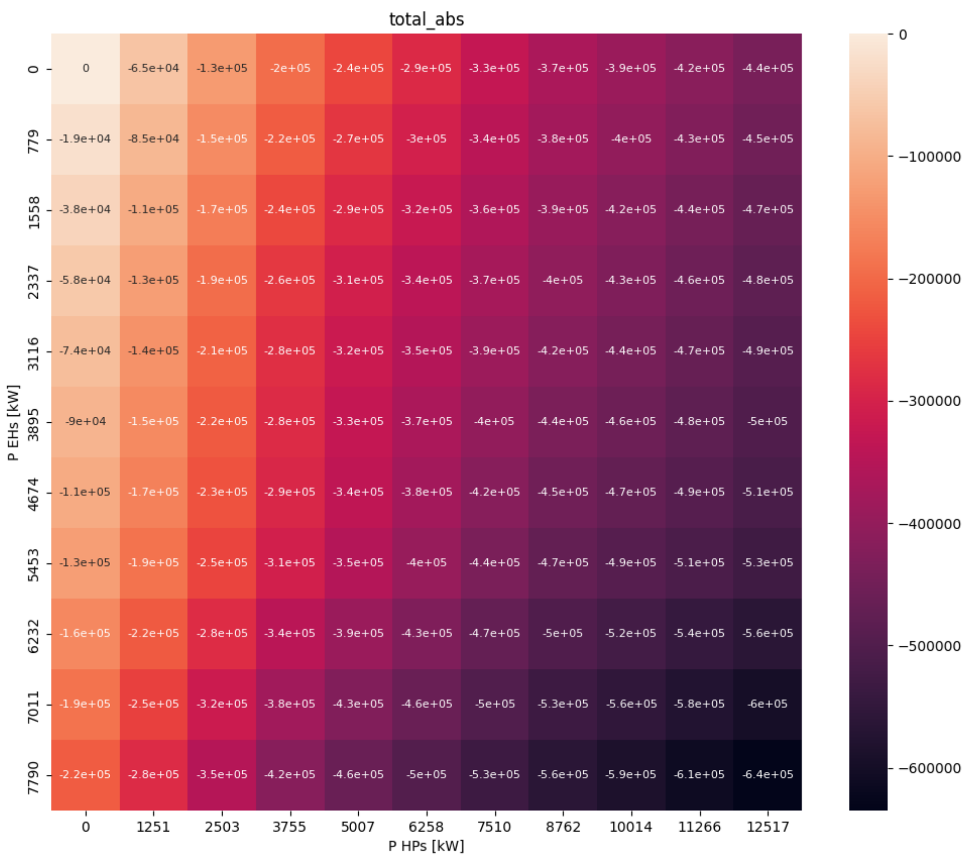


Figure 27: Total cost matrix for different combinations of total controlled HPs and electric boilers.

## 2.7 Long-term evolution of flexibility and System Dynamics

The following will describe in detail the components of the System Dynamics (SD) model, whose purpose is to assess the long-term adoption of flexible devices and the share of these that are put at the disposal of the DSO. The SD methodology builds on theories of non-linear dynamics and feedback loops developed in mathematics, physics, and engineering [9] [10] [11], and was chosen for this study as it has been suggested and applied several times for the study of socio-technical transition processes (see [12] for a comprehensive review).

| **Reference Concept (*RC*)** | | **New Concept (*NC*)** | | **Flexible Concept (*FC*)** | |
|---|---|---|---|---|---|
| **Name** | **Explanation** | **Name** | **Explanation** | **Name** | **Explanation** |
| Oil Boiler | SH & DHW | Heat Pump | Both SH & DHW | Heat Pump flex | Both SH & DHW |
| Gas Boiler | SH & DHW | Oil & HP | Oil: 75%(SH & DHW) [1]<br>HP: 25%(SH & DHW) | Oil & HP flex | Oil: 75%(SH & DHW)<br>HP: 25%(SH & DHW) |
| Wood Boiler | SH & DHW | Gas & HP | Gas: 75%(SH & DHW)<br>HP: 25%(SH & DHW) | Gas & HP flex | Gas: 75%(SH & DHW)<br>HP: 25%(SH & DHW) |
| EH | SH & DHW | HP & ST | HP: SH<br>ST: DHW | HP & ST flex | HP: SH<br>ST: DHW |
| Oil & EH | Oil: SH<br>ST: DHW | Oil & ST | Oil: SH<br>ST: DHW | EH flex | SH & DHW |
| Gas & EH | Gas: SH<br>EH: DHW | Gas & ST | Gas: SH<br>ST: DHW | Oil & EH flex | Oil: SH<br>EH: DHW |
| Wood & EH | Wood: SH<br>EH: DHW | Pellet & ST | Pellet: SH<br>ST: DHW | Gas & EH flex | Gas: SH<br>EH: DHW |
| | | Pellet | Both SH & DHW | Wood & EH flex | Wood: SH<br>EH: DHW |

Table 9: Heating concepts used in the SD model

The SD model has been developed to assess the diffusion in the next decades of different heating technologies and PV systems in the residential sector. In Table 9 are reported the types of residential heating technologies considered in the model and their categorization in three concept groups: "*Reference Concept*" (RC), "*New Concept*" (NC) and "*Flexible Concept*" (FC). In the *Reference Concept* category are grouped the heating technologies that, as indicated in the "Model energy requirements of the cantons" (MoPEC), can't be installed anymore, as this would result in more than 90% of the building heating energy to be produced by fossil fuel or direct electric heating. In the *New Concept* category are the heating technologies that respect the MoPEC restrictions, which are taken from the MoPEC Standard Solutions [22]. In the *Flexible Concept* group, buildings providing flexibility to the DSO are collected; it comprehends electricity-based heating solutions that are either compliant with the MoPEC or not.

Figure 28 illustrates the possible changes that, according to the developed model, the different actors can make with regard to their heating technology. The actors (people with decision power on the considered building) in *RC* can choose to change their heating technology and adopt one of the solutions

[1] it is the Standard Solution 10, where it is suggested to have a fossil based heating technology for base load (covering 75 % of demand) and a HP for the rest.

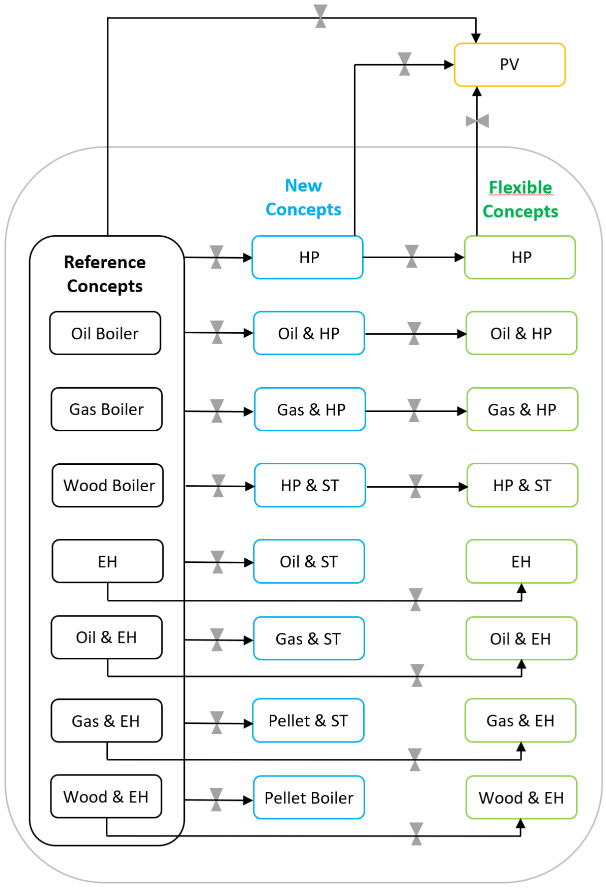


Figure 28: Possible concepts adoption paths

in the *NC* or *FC* groups. In the model, the adoption of a *NC* or *FC* concept can happen for one of two reasons: the end of the lifetime of the present technology or spontaneous adoption due to an advantageous perceived utility. As can be seen from the arrow direction in the figure, it is further assumed that once an actor has adopted a *NC* or *FC* technology, he cannot revert back to the previous concept group. At the same time, each actor in all three heating technology groups can spontaneously choose to install a PV panel, as better represented in Figure 29.

In Figure 29 is seen a Causal Loop Diagram (CLD) which represents a sample of the ODIS SD model with regards to the *Heat Pump*, *Heat Pump flex*, and PV adoption. A CLD is a visual representation of the relations between the main variables involved in the considered systems [23]. In a CLD there are arrows with a "+" or a "-", where the "+" sign indicates that the increase of the causal variable leads to an increase of the effect variable, while the "-" sign indicates an inverse proportion between the causal and effect variable. When the arrows link variable that form a circle, a causal loop is formed; it is indicated with a clockwise arrow containing a "*R*" or a "*B*". The "*R*" indicated a reinforcing loop, meaning that the increase of one variable leads to the change of a second variable, whose change leads to the increase of the first variable considered; the "*B*" indicates a balancing loop, meaning that the increase of one variable finally brings to the decrease of the same variable, leading to system stability. CLDs are useful to qualitatively comprehend how the most important variables in the modelled system interact, capturing their nonlinear behavior and feedback loops.

Loops *R1*, *R2* and *R3* represent the reinforcing loops due to peer effect, which is an indication of the social attractiveness of a given technology: the higher number of actors that have already adopted a given solution, the higher the social attractiveness for possible new adopters. Reinforcing loops *R4* and *R5* capture the dependence between the amount of flexibility providers and the total economic and GHG savings, that will increase perceived economic and green utility of *Heat Pump flex*. Reinforcing

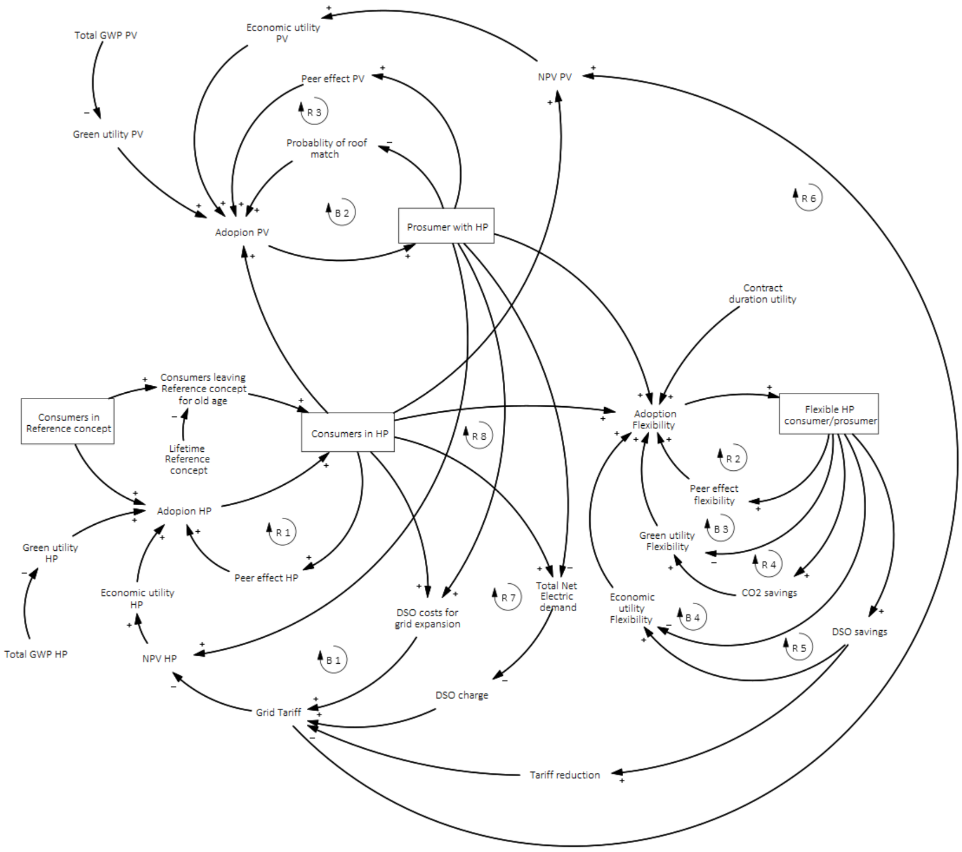


Figure 29: Causal Loop Diagram (CLD) of the SD model

loops *R6* and *R7* are two slides of the same coin, representing how the diffusion of electricity-based technology affects the electricity price. *R6* is known as the “*Death Spiral*” [24]: the higher the PV adoption, the lower the electricity demand from the DSO, whose costs remain, on the other hand, almost constant; so, the DSO is forced to increase the final electricity price, making the PV adoption choice more economically attractive. *R7* represent the same mechanism translated to heat pumps adoption, which finally brings a decrease to the electricity price. Feedback loops *B1* and *R8* represent the other long-term effects of massive HP and PV adoption; a high penetration of these technologies will force the DSO to act on the grid to reinforce it [25], and consequently increase the electricity price, which decreased the HP economic attractiveness and increases PV economic attractiveness. *B2* simply represents a boundary condition, being the total share of roofs suitable for PV installation constant, the higher the number of PV installed, the lower the probability of the remaining roofs to be adequate for future PV adoption. *B3* and *B4* capture the relation between the size of the flexibility pool and the incremental economic and environmental gains it provides; when increasing the total actors in *Flexible Concept*, the economic and GHG savings due to the single actor decrease, which leads to lower economic and green attractiveness.

### 2.7.1 Data Acquisition

The data used to model the initial condition of the building stock is all publicly available. Data from three different sources are collected for all residential buildings in the AMB area:

- Data from [26]: this database contains information on currently installed PV plants. For each plant, the nominal power is provided, as well as the year of installation.

- Data from [27]: this database is used to estimate the PV potential in the area considered. For each building, the roof is divided into sub-surfaces, which are classified based on their adequacy for PV installation. There are five different categories, which go from 1, the lowest adequacy, to 5, the highest. As later explained, the PV potential will be expressed as the share of the roof area with a score equal to or higher than 3.
- Data from the Register of Buildings and Dwellings (RBD) [28]: this database provides the heating technology, construction period, size, and type of a building.

These databases are used to for the categorization of the different building archetypes, as reported in Table 10.

| **Size [$m^2$]** | **Type** | **PV Presence** | **Construction Period** |
|---|---|---|---|
| < 60 (A)<br>60-120 (B)<br>> 120 (C) | Single Family House (SFH)<br>Dual Family House (DFH)<br>Multi Family House (MFH) | PV yes<br>PV no | < 1920<br>1920 - 1945<br>1945 - 1960<br>1961 - 1970<br>1971 - 1980<br>1981 - 1990<br>1991 - 2000<br>2001 - 2010<br>> 2010 |

Table 10: Categories that define the single building archetype

In order to compute the space heating demand for each building archetype, the study [16] is used. It is a study of the building stock of Canton Ticino, that correlates the specific annual space heating consumption of buildings, expressed in $kWh/m^2y$, with the building construction period. In the model, four levels of specific space heating loads are used to represent the building stock energy efficiency:

- Very Low – the weighted average of the specific space heating demand of residences built before 1960 is 145 $kWh/m^2y$.
- Low – the weighted average of the specific space heating demand of residences built between 1960 and 1985 is 105 $kWh/m^2y$.
- Moderate – the weighted average of the specific space heating demand of residences built between 1985 and 2010 is 65 $kWh/m^2y$.
- High – the weighted average of the specific space heating demand of residences built after 2010 is 15 $kWh/m^2y$.

Based on this categorization, the residential stock of the municipalities served by AMB is represented in Figure 30. Moreover, the space heating demand is adjusted with the coefficients in Table 11, which take into account the presence of common areas in different building types.

The residential building stock evolves due to the renovation of existing buildings, demolition of old buildings, and construction of new ones, as illustrated in Figure 31. The average values for Switzerland are assumed in this study: a renovation rate of 1% [29], and a demolition rate of 0.4% [30], while the construction rate is computed considering the total residential stock evolution of the last ten years [31] and the demolition rate. For the sake of simplicity, it is assumed that the buildings in *Very Low* category are demolished first, and only if there are no more *Very Low* buildings, the *Low* and *Moderate* are demolished. Moreover, only evolution towards more efficient construction is considered, and newly constructed buildings fall all under the *High* category.

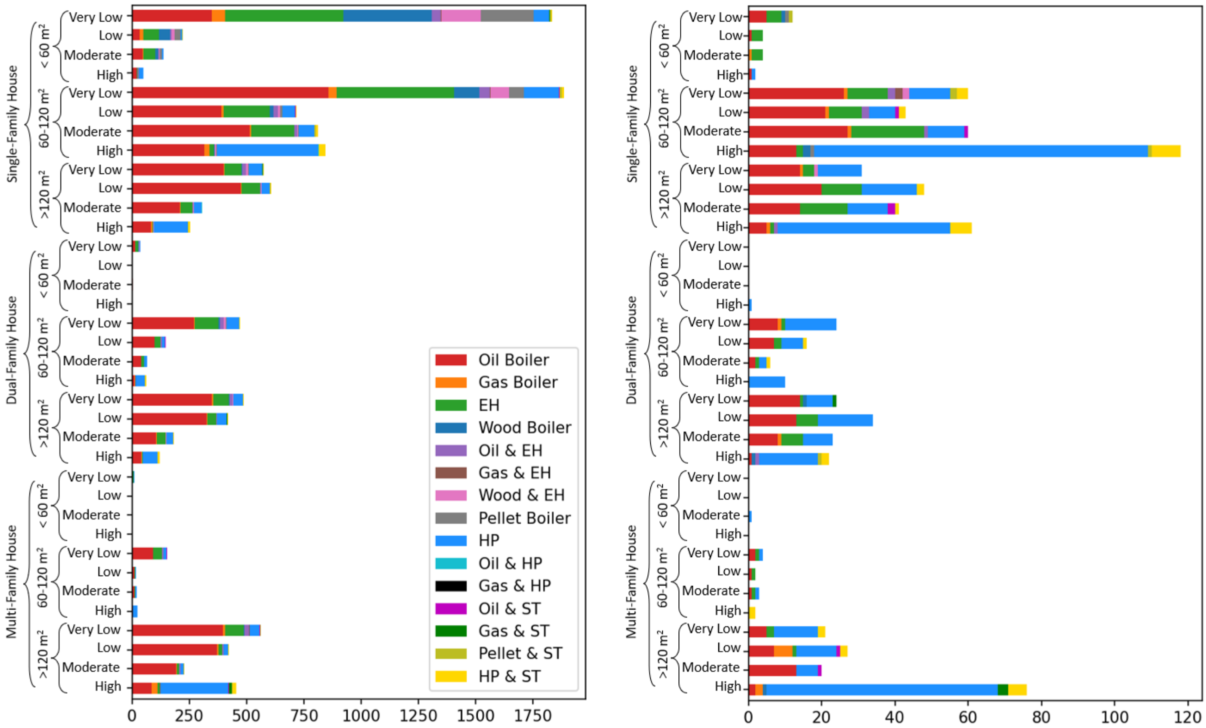


Figure 30: AMB residential stock (number of buildings on the x-axis) in 2023 categorized by Size, Type, Energy Efficiency, and PV presence (*PVno* on the left, *PVyes* on the right)

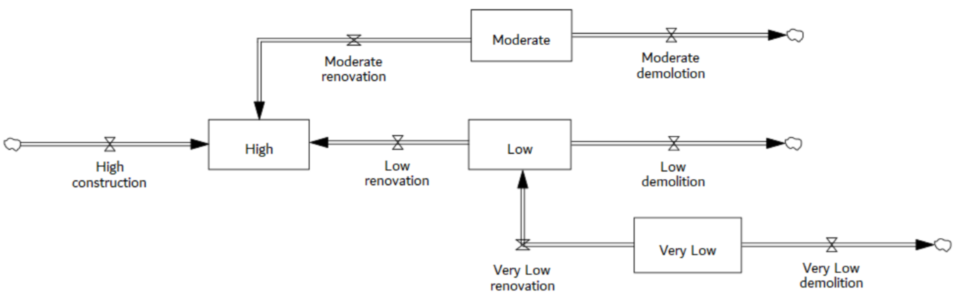


Figure 31: Construction, demolition, and renovation mechanisms in the modelled building stock

In order to estimate the initial state of building stock by *Size* and *Type* in the new construction, data from RBD is used, and Figure 32 shows the evolution of the new constructions based on their *Size* and *Type*; it is assumed that the trend represented in the figure will continue in the following decades. The annual hot water demand is computed for each building archetype considering the average hot water consumption of 40 l/day/person, average occupants per dwelling (Table 12), and the average number of 6.4 dwellings in the MFH of Canton Ticino [32]. Finally, the annual appliances' demand considered for each dwelling is 1400 $kWh/y$ [33], while light load density is 8.3 $kWh/m^2y$ [34].

### 2.7.2 Model driving equations

As illustrated in the CLD in Figure 29, there are many factors considered in the SD model to compute the adoption of a given heating technology. In fact, the adoption of *NC* is dependent not only on the building characteristics, meaning, as explained in Section 2.7.1, its *Thermal Efficiency*, *Size*, *Type* and whether it has a PV installed (all these characteristics define what will be called building "*archetype*"),

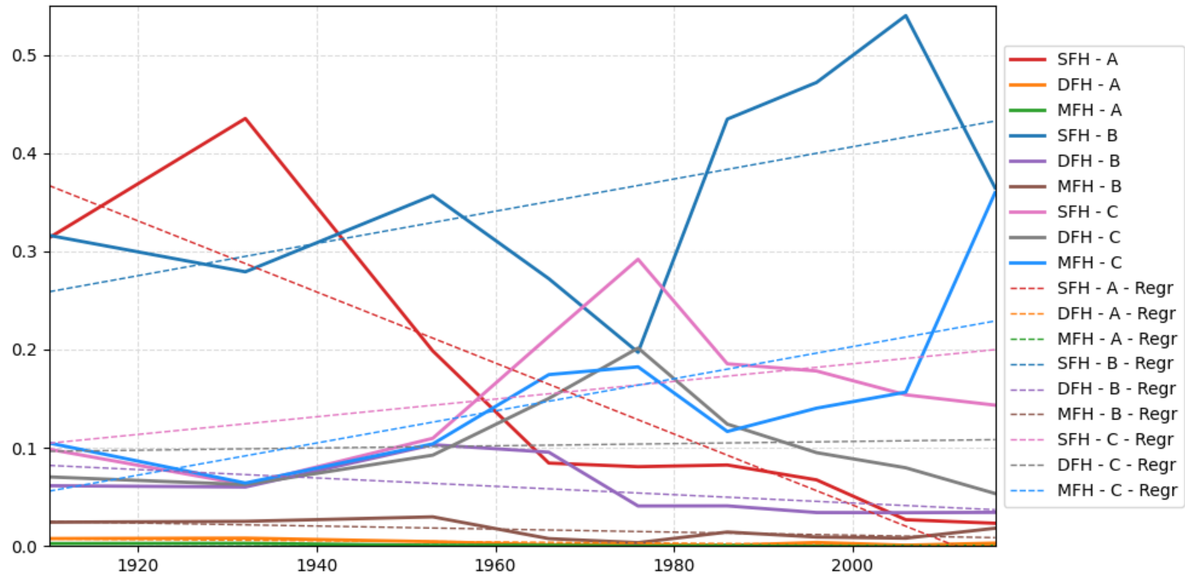


Figure 32: Building categorised by Size and Type shares evolution

but also the economic, environmental and social attractiveness of the possible new heating technology. The adoption of a *New Concept* $n$, for each building archetype $i$, and from each *Reference Concept* $rc$, is computed as:

$$a_{n,rc,i} = (C_{rc,i} - CNC_{n,rc,i}) \times SP_{n,rc,i} \times PRM_{n,i} \tag{15}$$

Where $C_{rc,i}$ are the consumers in each $rc$ and building archetype; $CNC_{n,rc,i}$ are the consumers in each $rc$ and building archetype not willing to change their present heating technology, computed as:

$$CNC_{n,rc,i} = C_{rc,i} \times (1 - u_{n,rc,i}) \tag{16}$$

Where $u_{n,rc,i}$ is the perceived utility of switching from concept $rc$ to $n$. $SP_{n,rc,i}$ is the share of preferences:

$$SP_{n,rc,i} = \frac{1}{1 + e^{-\beta(u_{n,rc,i} - urc_{rc,i})}} \tag{17}$$

$$urc_{rc,i} = \frac{1}{N}\sum_{n=1}^{N} u_{n,rc,i} \tag{18}$$

where $N$ is the total number of concepts that can be adopted starting from $rc$, and $urc_{rc,i}$ is the average utility of the *New Concept* for each *Reference Concept* and building archetype. $PRM_{n,i}$ is the probability of roof match and it is different from one just for the HT comprehending solar thermal collectors. It is computed starting from the share of suitable roofs ($ssr$) (Table 13), obtained from the data collected as reported in Section 2.7.1, as the ratio between the total roofs area that have a "Good" (category 3 in the database) or higher adequacy to solar installations. The $ssr$ is then subtracted from the share of buildings that have already installed a PV or ST collector.

$$PRM_{n,i} = ssr - \frac{Buildings\ with\ PV\ or\ ST_i}{Buildings_i} \tag{19}$$

The utility of each possible choice is computed as:

$$u_{n,rc,i} = euw \times eu_{n,rc,i} + guw \times gu_{n,rc,i} + pec \times pe_n \tag{20}$$

Where $euw$, $guw$ and $pec$ are the economic utility weight, the green utility weight and the peer effect coefficient, respectively, which are all found in the model calibration process with historical data. The peer effect $pe_n$ is a representation of the perceived social utility of a possible choice and is computed as the ratio between the buildings that have already adopted the considered *New Concept* and the total residential buildings.

$$pe_n = \frac{Buildings_n}{Total\ buildings} \tag{21}$$

The perceived economic utility of the consumers in each building archetype is expressed as a function of the Net Present Value divided by the number of dwellings in that building type ($d_i$), considering the total variable costs of both the *Reference Concept* ($TRCVC_{rc,i}$) and the *New Concept* one ($TCNVC_{n,i}$), the installation costs of the *NC* ($IC_{n,i}$) and its initial grant ($IG_{n,i}$):

$$eu_{n,rc,i} = (TRCVC_{rc,i} - TCNVC_{n,i} - IC_{n,i} + IG_{n,i})/d_i \tag{22}$$

Each $NC$ or $RC$ concept is a combination of one or two heating technologies ($t$), whose data are collected in Table 17. So, the installation cost is computed as the sum of the cost per kW installed ($C_t$) times the capacity installed ($Cap_{t,i,n}$) per each technology used, while the initial grant is computed considering both the initial absolute grant ($IAG_t$) and the grant per kW installed ($G_t$):

$$IC_{n,i} = \sum_t C_t \times Cap_{t,i,n} \tag{23}$$

$$IG_{n,i} = \sum_t (G_t \times Cap_{t,i,n} + IAG_t) \tag{24}$$

Where the capacity installed for each technology used in a new concept is given by the ratio of the demand for that technology in the considered building archetype ($D_{t,i,n}$) and the equivalent full load hours of that technology ($EFLH_t$):

$$Cap_{t,i,n} = \frac{D_{t,i,n}}{EFLH_t} \tag{25}$$

$TRCVC_{rc,i}$ and $TCNVC_{n,i}$ are computed considering the efficiency of the technology used ($Eff_t$), the cost of the carrier used by that technology ($CC_t$), its annual operation and maintenance costs ($OM_t$) and its lifetime ($Lifetime_t$), so that the present value is computed considering the interest rate ($r$):

$$TCNVC_{n,i} = \sum_t \left( \left( \frac{D_{t,i,n}}{Eff_t} \times CC_t + OM_t \times Cap_{t,i,n} \right) \times \frac{1 - \frac{1}{(1+r)^{Lifetime_t}}}{r} \right) \tag{26}$$

$$TRCVC_{rc,i} = \sum_t \left( \left( \frac{D_{t,i,rc}}{Eff_t} \times CC_t + OM_t \times Cap_{t,i,rc} \right) \times \frac{1 - \frac{1}{(1+r)^{Lifetime_t}}}{r} \right) \tag{27}$$

It is important to notice that the carrier used can also be electricity, whose cost changes endogenously in the model, as explained in more detail in Section 2.4. Moreover, since in the building archetypes the presence of PV is considered, if the considered building already has a PV installed, solutions such as *Heat Pump* and *HP & ST* will have a higher economic utility, being part of the electricity available by self-consumption at no cost.

The green utility is computed with a similar procedure, as a function of the Total Global Warming Potential (GWP) of the possible *New Concept* adoption compared to the *Reference Concept* one:

$$gu_{n,rc,i} = (TRCVE_{rc,i} - TCNVE_{n,i} - IE_{n,i})/d_i \tag{28}$$

$$TCNVC_{n,i} = \sum_t \left( \frac{D_{t,i,n}}{Eff_t} \times CE_t \times Lifetime_t \right) \tag{29}$$

$$TRCVC_{rc,i} = \sum_t \left( \frac{D_{t,i,rc}}{Eff_t} \times CE_t \times Lifetime_t \right) \tag{30}$$

$$IE_{n,i} = \sum_t E_t \times Cap_{t,i,n} \tag{31}$$

Where $E_t$ and $CE_t$ are the emissions related to the capacity installed of the selected technology and the ones related to its carrier, respectively.

The process to compute the consumers adopting a PV ($apv_{h,i}$) plant is similar to the one for heating concepts. In this case it is dependent on the building archetype and its heat source ($h$) which classifies the buildings based on the amount of heating demand coming from electricity-driven technologies (Table 9). So, as the adoption of a given heating concept is affected by the presence of a PV, also the possible PV adoption is affected by the actual heating concept, since the higher the electricity demand, the higher the PV Net Present Value.

$$apv_{h,i} = (C_{h,i} - CNC_{h,i}) \times SP_{h,i} \times PRM_{h,i} \tag{32}$$

$C_{h,i}$ and $CNC_{h,i}$ represent the total consumers and the consumers not willing to adopt PV in a building archetype and heating source, respectively. $SP_{h,i}$ and $PRM_{h,i}$ are the share of preference and the probability of roof match, computed as explained above for Solar Thermal installations. In order to compute the NPV and the GWP of the possible PV installation, the PV size is computed based on the following assumptions. The average portion of roof suited for PV installation is equal to 0.7 for SFH and 0.7*0.6 for DFH and MFH [35]. Then, from the data collected as reported in Section 2.7.1, the average roof size is computed for each building archetype (Table 14). Considering the square meters needed to install 1 kWp and an annual energy production of 1160 kWh/kWp [36], the maximum kWp of PV installed is computed for each building archetype. Moreover, it is assumed that the installed capacity is also a function of the electricity demand of the building considered, so a minimum Self-Consumption (SC) degree of 15% is adopted; this is the value that allows to have the total kWp installed (computed in the model) equal to the real value (taken from [27]) for the year 2023. Starting from this data and the annual electricity demand of each building (computed considering the light and appliances demand, and the electricity demand for heating based on the building heat source) the capacity installed corresponding to the minimum SC is computed, using [37] and considering no storage. So:

- If the capacity corresponding to the minimum SC degree is higher than the maximum capacity based on the roof size, PV covering all the available roofs is installed, and a new (higher) SC degree is computed for the building considered.
- If the capacity corresponding to the minimum SC degree is lower than the maximum capacity based on the roof size, that capacity is installed, and not all the area available on the roof is exploited.

In this way, it is possible to compute the PV economic utility, considering the electricity price and incentives for PV, reported in Tables 15 and 17; while, regarding the green utility, the GHG emissions saved are computed considering the average emissions for electricity from the grid (see Table 17).

As for the previous two adoption processes, the *Flexible Concept* adoption for each building archetype is computed with the equation:

$$af_{f,i} = (C_{f,i} - CNC_{f,i}) \times SP_{f,i} \tag{33}$$

Where $C_{f,i}$ and $CNC_{f,i}$ represent, respectively, the potential buildings that can provide flexibility and buildings not willing to provide it, categorized on the heating technology to be controlled by the DSO ($f$) and the building archetype ($i$). The perceived utility is computed considering not only economic and environmental importance but also the utility associated to the flexibility contract duration with the DSO [38], here assumed to be of 1 year.

$$u_{f,i} = (euwf \times euf_{f,i} + guwf \times guf_{f,i} + cuwf \times cuf_{f,i}) \times pe_f \times pec \tag{34}$$

Where the economic utility weight ($euwf$), the contract utility weight ($cuw$) and the green utility weight for flexibility ($guwf$) are taken from [38]. In this case the peer effect for flexibility is computed considering all the buildings providing flexibility, independently from the heating technology controlled by the DSO.

The green utility ($guf_{f,i}$) represent the total GHG saved due to the controlled device of the building considered. It is computed from the results of the optimization described in Section 2.4, where the total GHG saved are expressed as a function of the total power controlled from HPs and EHs; the total emissions saved are divided between all the buildings providing flexibility proportionally to the installed power of the controlled device. From the optimization process, also the total DSO savings are computed. In this case, it is assumed that just part of these savings is used as an incentive to attract new flexibility providers, while the remaining part is redistributed to all the DSO consumers, reducing the electricity price. So, the money offered to new flexibility providers is computed in terms of monthly CHF per kW provided to DSO control. Finally, Figure 33 and Figure 34 represent the perceived economic and contract utility corresponding to the CHF/month offered and the contract duration, readapted from [38].

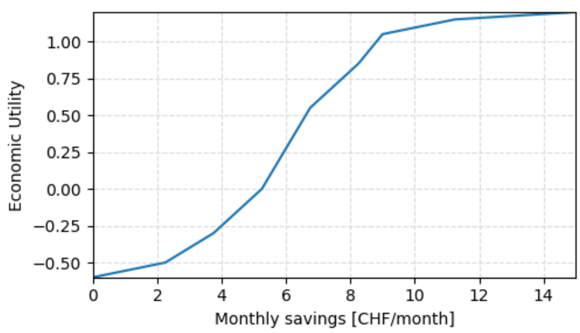


Figure 33: Perceived economic utility

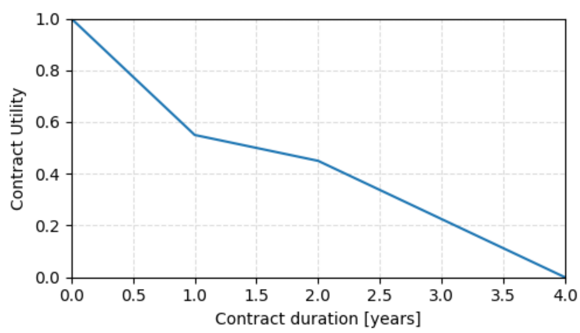


Figure 34: Perceived contract utility

Moreover, the electricity price for the final consumer is computed endogenously in the model, as a function of different parameters:

$$p = e_p + c_{TSO} + c_{DSO} + t_c + t_f \tag{35}$$

Where $e_p$, $c_{TSO}$, $t_c$ and $t_f$ represent the cost due to energy production, the TSO charge, the cantonal tax and the federal tax respectively; these values, reported in Table 16, are kept constant and equal to the values of 2023 in the future. On the other hand, it is assumed that the DSO charge ($c_{DSO}$) changes as a function of the total DSO costs and the total final demand.

$$c_{DSO} = \frac{DSO\ Costs}{Total\ Final\ Demand} \tag{36}$$

The total DSO costs are computed for the year 2023 considering the DSO charge and total final demand of the same year. Moreover, this cost is updated in the model considering the increasing costs for the DSO necessary to upgrade the grid because of heat pumps and PV penetration ($C_{GU}$), and the savings due to final consumers providing flexibility ($S_{flex}$). It is assumed that half of the savings due to flexibility is used to reduce the electricity price, while the other half is redistributed to flexibility providers. The $C_{GU}$ are computed considering the HP and PV capacity installations, the average cost per kW installed taken from [25] and the classification of cities in the AMB district from [39].

$$DSO\ Costs_{2023} = c_{DSO,2023} \times Total\ Final\ Demand_{2023} \tag{37}$$

$$DSO\ Costs = DSO\ Costs_{2023} + C_{GU} - 0.5 \times S_{flex} \tag{38}$$

### 2.7.3 Model Calibration

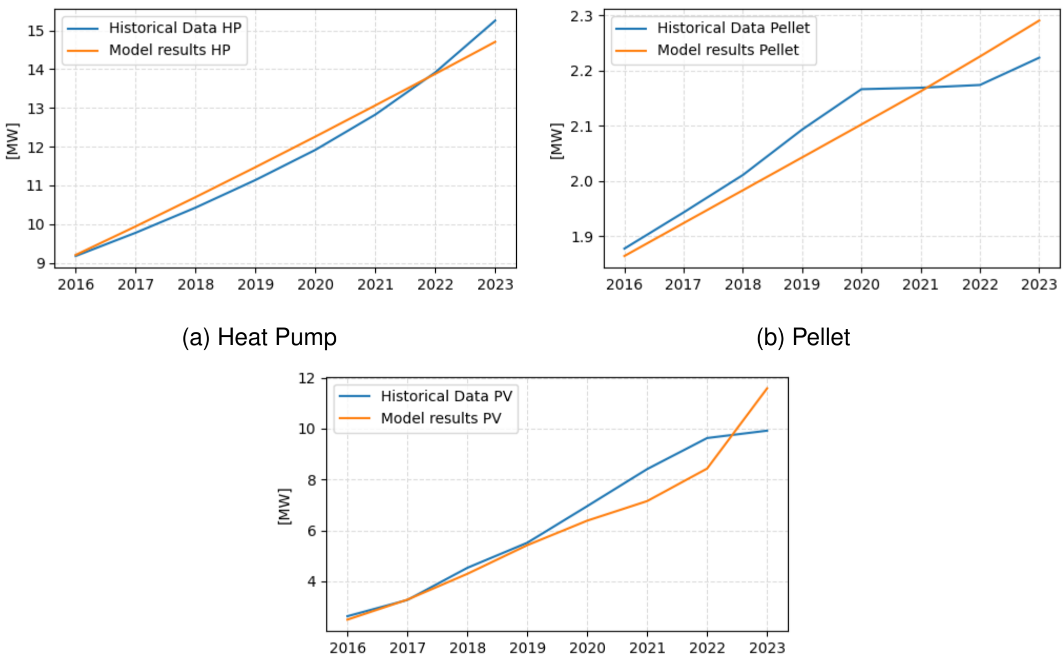


(a) Heat Pump



(b) Pellet



(c) PV panel

Figure 35: Results of the calibration process for the total HP, Pellet and PV capacity

Before evaluating how the system considered to evolve until 2050, it is necessary to capture the system's behavior. With this as a goal, a fundamental step in building this system dynamics model is its calibration with historical data of the AMB serviced area. The calibrated variables are the different coefficients involved in the adoption decision of both heating technologies and PV panels, namely $euw$, $guw$, $pec$, $euw_{PV}$, $guw_{PV}$ and $pec_{PV}$. The historical data used for the calibration are:

- Total PV installed capacity [kW]: these values are collected from [26], where the installation year of the PV plant and its nominal capacity is provided.
- Total heat pump installed capacity [$kW_{th}$]: these values aren't directly available in the Residential Buildings and Dwellings database, so the values of the yearly HP sold [40] is used to scale back the 2023 data for the AMB serviced area.
- Total pellet boiler installed capacity [$kW_{th}$]: these values aren't directly available in the Residential Buildings and Dwellings database, so the values of the overall Swiss pellet capacity installed in the residential sector [41] is used to scale back the 2023 data for the AMB serviced area.

During the calibration process, the variables mentioned above are changed to find the values that minimize the Normalized Root Mean Square Deviation (NRMSD) between the historical data and the same parameters computed in the model. In order to ensure the convergence of the calibration process, reasonable bounds for each utility weight are considered so that each variable cannot reach a null value. This means that after initializing the model with data from 2016, the following seven years (until 2023) of the simulation have a resemblance with the historical data that was deemed sufficient. It can also be noted that the objective of the model is to provide basic insights into the possible mid-to-long-term evolution of the system and its resulting flexibility potential rather than quantitatively predicting the annual fluctuations (inclines and declines) for each year until 2050. That is to say the objective of the calibration process was to resemble as much as possible the historical data, while prioritizing the replication of the overall trend, rather than specific annual fluctuations. Figure 35 shows the results of the calibration process.

# 3 Results and discussion

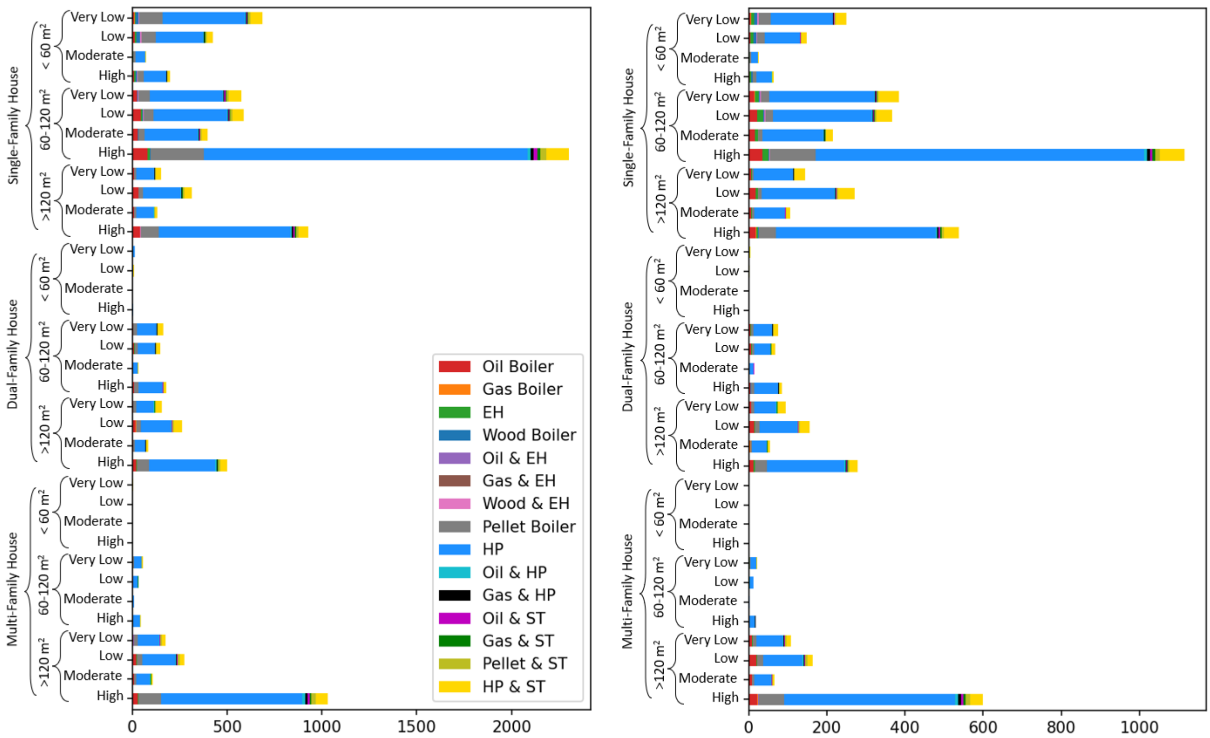


Figure 36: AMB residential stock in (number of buildings on the x-axis) 2050 categorized by Size, Type, Energy Efficiency and PV presence (*PVno* on the left, *PVyes* on the right)

Figure 36 shows the final heating technology for each building archetype. Compared to the residential building situation in 2023, shown in Figure 30, the first important difference is the higher presence of energy efficient buildings; this is affected by three factors: the renovation rate of 1%, the assumption that the new constructions are in the *High* category and the assumption that the demolished building are from the *Very Low* category.

Two technologies are dominant in the 2050 results: heat pumps and pellet boilers. In fact, the *New Concept* solutions that are based on these technologies, namely *Heat Pump*, *Pellet*, *HP & ST* and *Pellet & ST*, are the most convenient from all the three dimensions involved in the decision process. Moreover, heat pumps have a significantly higher economic and social attractiveness: this results in a final share of solutions based on heat pumps of 76%, followed by the share of solutions based on pellet boilers (10.5%). It is important to notice that this model does not pretend to predict the future and that its presented results are based on the assumption that the current incentive scheme will not change, which is a scenario that may or may not occur.

Following the current installation trend, the number of buildings with a PV installed continues to increase until 2050, with a final share of buildings equipped with PV of 34%, which is significantly higher than the 6.5% of 2023. Moreover, there are differences in final heating technologies shares between prosumers (*PVyes*) and consumers (*PVno*): in the SD model the choice to install a PV and the choice of the heating technology are affected by the heating technology already installed and the presence of PV, respectively. Because of the higher electricity consumption, consumers with a heat pump have a higher economic incentive to install PV panels, and, because of the free electricity available from their own plant, prosumers have a higher economic incentive to install a heat pump. For these reasons, 36% of buildings with a heat pump also have a PV installed, while just 28% of building heated with pellet boilers have.

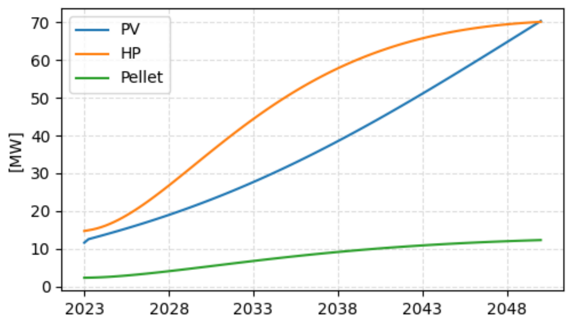


Figure 37: Total installed capacities

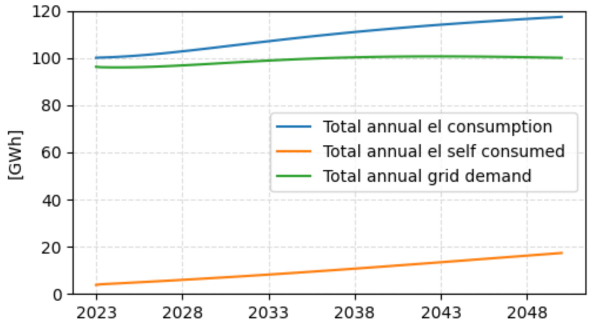


Figure 38

Figure 37 represents the total installed capacities in the AMB serviced area for the three technologies of interest: heat pumps, pellet boilers, and PV. There is a clear difference in the adoption speed between heating technologies and PV. This is because, following the line of the MoPEC, consumers that install a new heating system are forced to adopt one of the *New Concept* solutions. So, in the model, once heating technologies in a *Reference Concept* reach the end of their lifetime, they are substituted most of the time with heating systems based on heat pumps and pellet boilers. On the other hand, the penetration of solar PV is just based on the spontaneous adoption of consumers, which, considering that the actual incentive scheme will remain unchanged in the future, will continue without abrupt changes such as the ones in the heating technologies penetration.

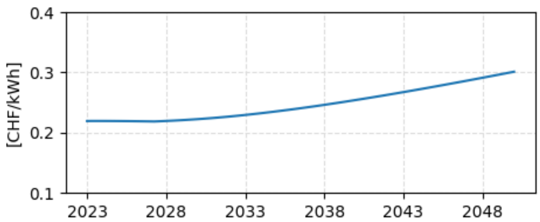


Figure 39

In Figure 39 is shown the evolution of electricity price, which changes in the model according to the description in Section 2.7.2. Its trend is affected by two mechanisms:

- The total final electricity bought from the grid is the first important factor: considering constant fixed costs for the grid, if it increases the final electricity price for the residential sector decreases. In the model, the demand increase due to HP penetration and the demand decrease due to PV penetration counterbalance each other. These factors can be seen in Figure 38 and represent the feedback loops *R7* and *R6* in Figure 29.

- The costs for the DSO related to the grid upgrading due to the higher HP and PV penetration shown in Figure 37. These costs are considered from 2028, affecting the electricity price mainly after 2030.

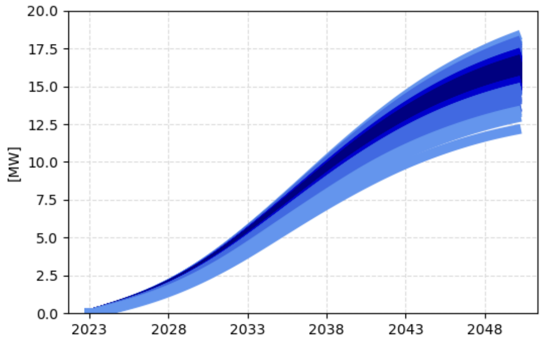


(a) Total capacity controlled by the DSO

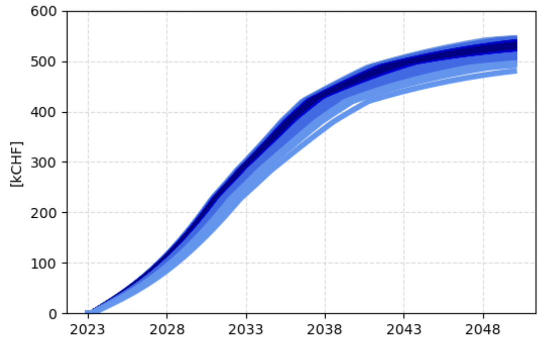


(b) Total DSO savings related to HT control

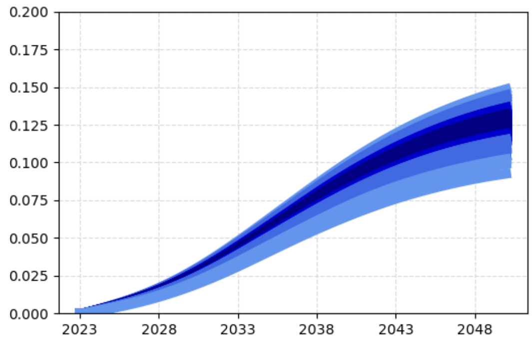


(c) Peer effect flexibility

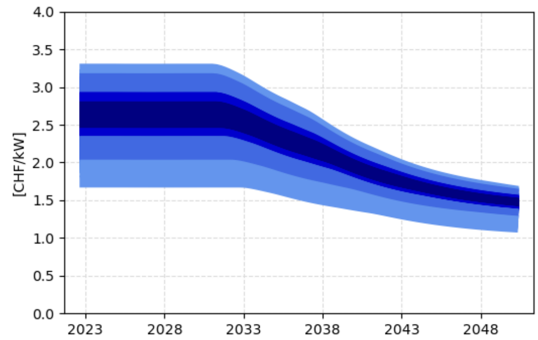


(d) Money offered by the DSO to the flexibility providers

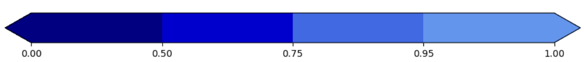


(e) Confidence intervals

Figure 40: Main results related to flexibility providers.

Figure 40 shows the main results in terms of flexibility provided to the DSO and its monetary implications. To evaluate how the compensation offered to flexibility providers affects the total final adoption, the simulation is repeated, varying the percentage of savings used to decrease the final consumer electricity price, with this parameter varied between 35% and 65% in a Monte Carlo simulation. If this percentage increases, the savings used to attract new flexibility providers decreases.

In Figure 40a and 40b are represented the total HPs capacity controlled by the DSO and its savings, respectively. Both variables have a clear s-shaped trend, which reflects the results reported in Section 2.4. Initially, the savings for the DSO increase linearly with the total capacity controlled, but between 2030 and 2035 the capacity controlled is high enough to have a decrease in the marginal savings, so that the economic incentive offered to flexibility providers decreases, bringing a lower *Flexible Concept* adoption. The final annual savings for the DSO are estimated using the results represented in Figure 47 and vary between 480 kCHF and 550 kCHF.

Figure 40c shows how these changes affect the peer effect of flexibility: in 2050, the total percentage of buildings providing flexibility varies between 8.5% and 15%, when the share of savings redistributed to all is set to 65% and 35%, respectively. This corresponds to an annual amount of avoided emissions due to flexibility control varying between 350 and 440 tons of $CO_2$, evaluated with the results reported in Figure 48. Instead, in Figure 40d is represented the evolution of the offered compensation per kW controlled by the DSO. When the share of savings redistributed to all is higher, the offer for the final consumer is lower, leading to a lower flexibility adoption. Figure 40d is also representative of the decrease in the marginal savings for the DSO once the total controlled capacity reaches an enough high value. Finally, due to the low impact of DSO savings compared to the overall annual DSO expenses computed in the model, the final electricity price doesn't change significantly.

The analysis just described allowed to identify one key leverage point that affects deeply the way the system considered will evolve. This element is the minimum self-consumption. As described in Section 2.7.2, the minimum self-consumption was set to 15%, which is the value that allows to have the total kWp installed (computed in the model) equal to the real value. In fact, a high PV penetration, besides helping to reduce the overall greenhouse gas production from the electricity sector, could also bring problems to the grid, such as significant over-voltage and over-loading issues and changes in the reactive power balance. For these reasons, it is not excluded that in the future years a norm with the aim of increasing the self-consumption for new PV installations will be enacted. In this case study, it is considered that in the year 2030 a new law will act in this direction, and, in order to understand how the system considered could react to such a change, a Monte Carlo analysis is performed, varying the minimum SC between 10% and 30% from the year 2030.

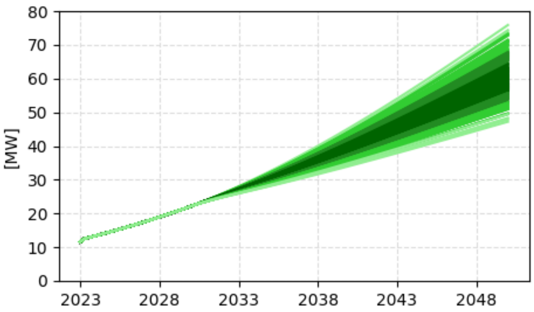


(a) Total PV capacity installed in MC analysis

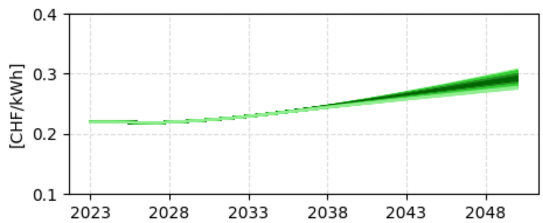


(b) Electricity price variation in MC analysis

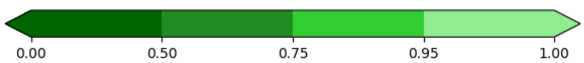


(c) Confidence intervals

Figure 41

As can be seen in Figure 41a, the main parameter affected by this change is the total PV installed capacity in the considered area: if the minimum self-consumption is set to a higher value, being the electricity demand constant over the years for each building archetype, the installed capacity will be lower. The DSO costs to upgrade the grid due to the higher PV penetration will change accordingly with the PV installed capacity and also the electricity price will be affected by such change in the law scheme, as shown in Figure 41b.

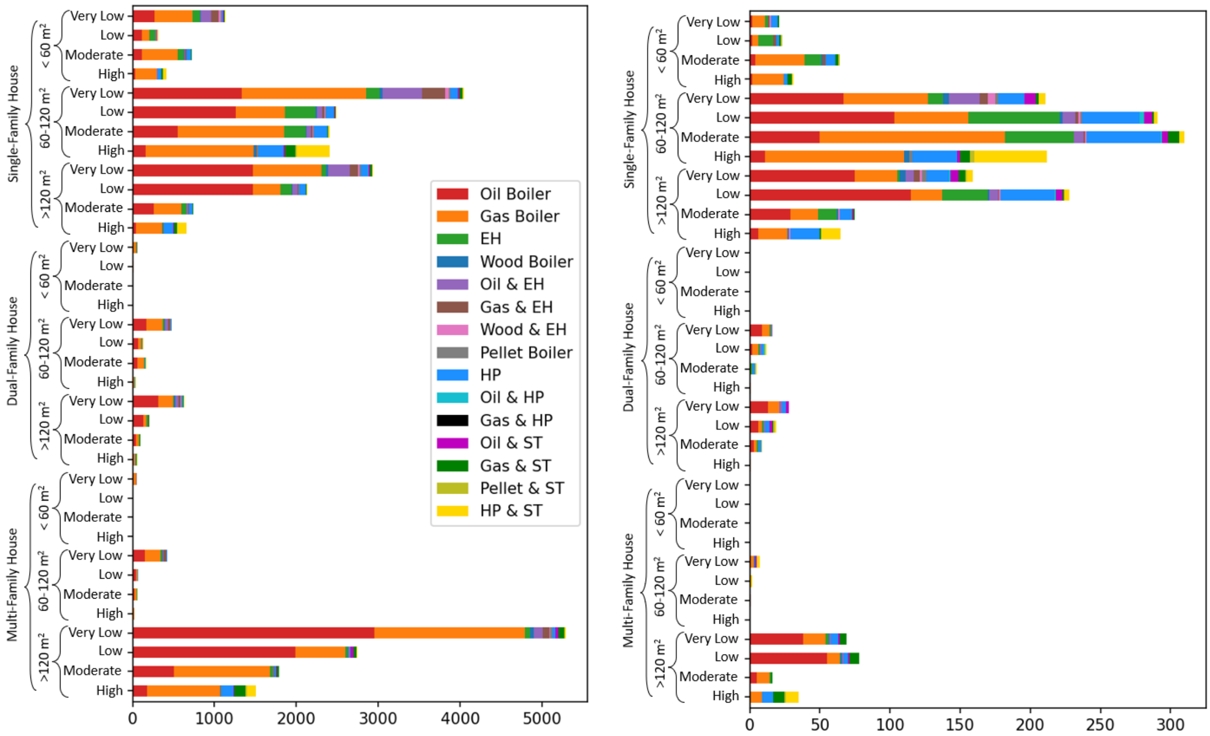


Figure 42: Geneve residential stock (number of buildings on the x-axis) in 2023 categorized by Size, Type, Energy Efficiency and PV presence (*PVno* on the left, *PVyes* on the right)

## 3.1 Replicability analysis

The techno-economically optimized savings for AMB, found through a data-driven approach and the development of a flexibility oracle, were implemented in the SD model in order to test the redistribution scheme remunerating the flexibility providers as well as reducing the electricity price for all residential customers. The SD model was also used to evaluate if the same business model could be replicated by another DSO, and how the adoption process of flexibility is affected by initial input conditions such as building archetype shares and policy schemes. To this end, the model developed for the AMB case study was used with new input data representing the state of the residential sector serviced by Services industriels de Genève (SIG), and a comparison between the results for the two DSOs is conducted. The data for Geneva buildings are collected following the procedure described in Section 2.7.1, while a summary of the existing policies for heating technologies and PV panels is presented in Table 17.

Figure 42 shows the building archetype shares at the beginning of 2023. Notably, there are two main differences compared to the initial AMB data (Figure 30): firstly, the initial share of buildings equipped with *Gas Boiler* is higher in Geneva, whereas there are fewer buildings with heating systems based on direct electric heaters, heat pumps, wood boilers, and pellet boilers. Secondly, Geneva has a much higher share of MFH (34%) compared to AMB (16%), due to its higher population density.

As illustrated in Figure 43, the final number of buildings with a heating technology based on heat pumps is higher in Geneva (80%) compared to the AMB area. This is attributed to the policy scheme implemented in the Geneva Canton, which is more stringent compared to Ticino. In particular, only heating systems fully based on renewable sources can be installed, meaning that only *Heat Pump*, *HP & ST*, *Pellet* and *Pellet & ST* are considered among the *New Concept* solutions modeled [42]. Furthermore, as reported in Table 17, the incentives guaranteed for pellet boilers are lower in Geneva than in Canton Ticino, resulting in a higher relative utility of *Heat Pump* and *HP & ST* concepts.

The policy scheme in the Geneva Canton also has a positive effect on the final PV adoption. Although

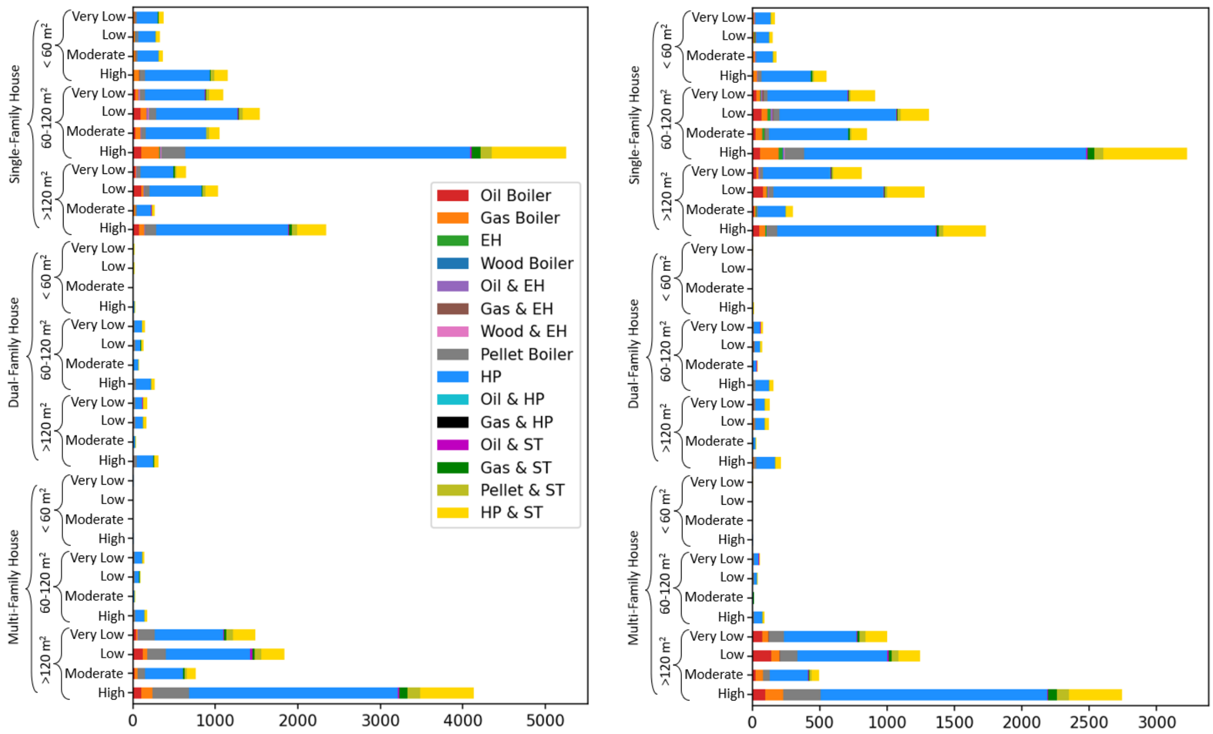


Figure 43: Geneve residential stock (number of buildings on the x-axis) in 2050 categorized by Size, Type, Energy Efficiency and PV presence (*PVno* on the left, *PVyes* on the right)

the incentives for PV installation are the same in the two Cantons, the feed-in tariff is higher in the Geneva case (see Table 15), leading to a higher economic utility and, consequently, a higher adoption. This higher feed-in tariff compensates for the fact that the economic utility is, on average, lower for MFH (as shown in Figure 44), even though the total NPV for MFH is higher since, in the model, the NPV is divided by the average number of dwellings per building type. For the same reason, also the total number of spontaneous adoptions of heating solutions in *New Concept* differs between the two case studies: the AMB serviced area has a higher share of SFH, resulting in a 11% higher share of spontaneous adoptions over total adoptions of new heating technology.

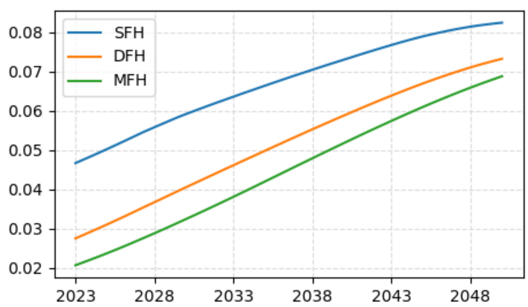


Figure 44: Average economic utility for PV adoption by *House Type*

The difference in the perceived economic utility between SFH and MFH also has a significant impact on the final share of consumers providing flexibility. Assuming the same share of savings due to flexibility providers used to attract new people allowing the DSO to control their heating device (50%), the amount of CHF offered monthly per kW controlled is the same for the two case studies. However, the average kW controlled for each dwelling of an MFH is lower compared to the power controlled in an

SFH, leading to a lower economic utility. Consequently, the final share of buildings with a controllable heating technology providing flexibility is 16% for the AMB serviced area and 13% for Geneva. As a result, the impact of electricity cost reduction due to flexibility providers is even lower in the Geneva case study than in the AMB one.

# 4 Conclusions

The ODIS project investigated how flexibility could be activated such as to reach a techno-economic optimum. Using a data-driven methodology to characterize and control flexibility in terms of the power system response to a given broadcasted control signal, the optimization of the energy purchased from the TSO leads to savings. In the considered case study of AMB, the data-driven forecaster demonstrated that there is economic potential for the DSO, where under the participation of the maximum considered penetration of HPs and EHs an annual cost reduction of 640 kCHF was generated, equivalent to a reduction of the overall energy and peak expenses of about 1.4 %.

However, careful attention needs to be paid to the redistribution of these economic gains as the amount of flexibility activated depends on the capacity and willingness of the device owners to put them under the control of the DSO. As can be seen from the SD model results, there is a tradeoff between the choice of using these savings to decrease the electricity price and using it to attract new flexibility providers, increasing the "flexibility pool". If the flexibility providers are compensated with a higher portion of these savings, the utility of adhering to a flexibility program grows, leading to a faster increase of the "flexibility pool". However, as the "flexibility pool" grows, a saturation point is likely to occur, after which additional flexible devices do not provide any more marginal savings (this is particularly true for the reduction in power peak costs, where the marginal efforts in terms of kWh to lower the monthly peaks increases as the peak decreases). At the same time, under the principles of fairness, the DSO should design a flexibility retribution scheme that is accessible to all flexibility device owners and might not deny participation even if such a saturation point has been reached. In this case, a potential way to ensure scalability and maintain the appeal to the flexible device owners could be to seek not only savings derived from the DSO-TSO energy and peak power tariff scheme but also revenues by offering the aggregated flexibility to third parties or directly accessing ancillary markets.

In addition, there are other important factors that affect the growth of the “flexibility pool”, such as the initial building stock characteristics and the policy approved by Cantonal and Federal governments to foster technologies based on renewable energy, which can’t be directly controlled by the DSO decisions based on its business plan. Nevertheless, these factors play a significant role in the ODIS System dynamics model results, as described in Section 3.1. In the Geneve case study, even though the initial share of heat pumps and pellet boilers is lower compared to the initial AMB situation, the final penetration of these technologies is higher due to the stricter law on new heating technologies installations in force in the Geneva Canton. At the same time, even though the final heat pump adoption is higher in Geneve, due to the higher MFH share, the share of buildings taking part in the “flexibility pool” is lower, resulting in lower DSO total savings.

# 5 Outlook and next steps

The ODIS project provides DSOs with a methodology to quantify economic benefits enabled by optimally controlling flexibility in their grid and how these could evolve over time, given a profit redistribution scheme for consumers. For the considered case study of AMB, under the maximum considered penetration of HPs and EHs scenarios, we have estimated an annual cost reduction of 640 kCHF, which is just a small portion of the overall energy and peak expenses (around 15 MCHF). The savings could be likely incremented considering control mechanisms other than ripple control. We envisage the following extension of the study:

- Considering smart-grid ready HPs. In this setting, we could steer HPs to both decrease and increase the consumption. This would increase the DSO's ability to shift consumption during low-tariff periods.
- Considering other flexible devices, such as EVs.

# 6 National and international cooperation

The project actively involves the sovra-regional DSO Azienda Elettrica Ticinese, the Azienda Multiservizi di Bellinzona and Hive Power. Some of the methods developed in ODIS will be tested in the ORCHESTRA 55136.1 IP-EE innosuisse project. The project outcomes also provided inputs to the international forum of the IEA EBC - Annex 82 - Energy Flexible Buildings Towards Resilient Low Carbon Energy Systems.

# 7 Publications

We are planning to publish an article on the flexibility estimation methodology and the evaluation of the control scheme. We also intend to publish an article on the factors influencing the growth of the flexibility pool.

# 8 References


[1] D. Fischer, T. Wolf, J. Wapler, R. Hollinger, and H. Madani, “Model-based flexibility assessment of a residential heat pump pool,” *Energy*, vol. 118, pp. 853–864, Jan. 2017. [Online]. Available: https://www.sciencedirect.com/science/article/pii/S0360544216315572

[2] F. Oldewurtel, D. Sturzenegger, G. Andersson, M. Morari, and R. S. Smith, “Towards a standardized building assessment for demand response,” in *52nd IEEE Conference on Decision and Control*, Dec. 2013, pp. 7083–7088, iSSN: 0191-2216.

[3] R. De Coninck and L. Helsen, “Quantification of flexibility in buildings by cost curves – Methodology and application,” *Applied Energy*, vol. 162, pp. 653–665, Jan. 2016. [Online]. Available: https://www.sciencedirect.com/science/article/pii/S0306261915013501

[4] G. Reynders, J. Diriken, and D. Saelens, “Generic characterization method for energy flexibility: Applied to structural thermal storage in residential buildings,” *Applied Energy*, vol. 198, pp. 192–202, Jul. 2017. [Online]. Available: https://www.sciencedirect.com/science/article/pii/S0306261917304555

[5] O. Corradi, H. Ochsenfeld, H. Madsen, and P. Pinson, “Controlling Electricity Consumption by Forecasting its Response to Varying Prices,” *IEEE Transactions on Power Systems*, vol. 28, no. 1, pp. 421–429, Feb. 2013, conference Name: IEEE Transactions on Power Systems.

[6] R. G. Junker, A. G. Azar, R. A. Lopes, K. B. Lindberg, G. Reynders, R. Relan, and H. Madsen, “Characterizing the energy flexibility of buildings and districts,” *Applied Energy*, vol. 225, pp. 175–182, Sep. 2018. [Online]. Available: https://www.sciencedirect.com/science/article/pii/S030626191830730X

[7] R. G. Junker, C. S. Kallesøe, J. P. Real, B. Howard, R. A. Lopes, and H. Madsen, “Stochastic nonlinear modelling and application of price-based energy flexibility,” *Applied Energy*, vol. 275, p. 115096, Oct. 2020. [Online]. Available: https://linkinghub.elsevier.com/retrieve/pii/S0306261920306085

[8] L. Yin and Y. Qiu, “Long-term price guidance mechanism of flexible energy service providers based on stochastic differential methods,” *Energy*, vol. 238, p. 121818, Jan. 2022. [Online]. Available: https://www.sciencedirect.com/science/article/pii/S0360544221020661

[9] J. W. Forrester, “Industrial Dynamics,” *Journal of the Operational Research Society*, vol. 48, no. 10, pp. 1037–1041, 1997. [Online]. Available: https://doi.org/10.1057/palgrave.jors.2600946

[10] G. P. Richardson, “Reflections on the foundations of system dynamics,” *System Dynamics Review*, vol. 27, no. 3, pp. 219 – 243, 2011. [Online]. Available: https://www.scopus.com/inward/record.uri?eid=2-s2.0-80053299467&doi=10.1002%2fsdr.462&partnerID=40&md5=45d17a928e3c4a84896bb3634b71e0c9

[11] J. Swanson, “Business Dynamics—Systems Thinking and Modeling for a Complex World,” *Journal of the Operational Research Society*, vol. 53, no. 4, pp. 472–473, Apr. 2002. [Online]. Available: https://www.tandfonline.com/doi/full/10.1057/palgrave.jors.2601336

[12] S. Selvakkumaran and E. O. Ahlgren, “Review of the use of system dynamics (SD) in scrutinizing local energy transitions,” *Journal of Environmental Management*, vol. 272, p. 111053, 2020. [Online]. Available: https://www.sciencedirect.com/science/article/pii/S0301479720309816

[13] “Home.” [Online]. Available: https://www.geo.admin.ch/

[14] F. S. Office, “Statistica degli edifici e delle abitazioni (dal 2009) | Fact sheet,” Oct. 2016. [Online]. Available: https://www.bfs.admin.ch/bfs/en/home/statistics/catalogues-databases/surveys.assetdetail.8797.html

[15] K. N. Streicher, P. Padey, D. Parra, M. C. Bürer, S. Schneider, and M. K. Patel, "Analysis of space heating demand in the Swiss residential building stock: Element-based bottom-up model of archetype buildings," *Energy and Buildings*, vol. 184, pp. 300–322, Feb. 2019. [Online]. Available: https://www.sciencedirect.com/science/article/pii/S0378778818325660

[16] L. Pampuri, N. Cereghetti, P. G. Bianchi, and P. Caputo, "Evaluation of the space heating need in residential buildings at territorial scale: The case of Canton Ticino (CH)," *Energy and Buildings*, vol. 148, pp. 218–227, Aug. 2017. [Online]. Available: https://www.sciencedirect.com/science/article/pii/S0378778816312920

[17] Brüttisellen-Zurich, "SIA-Shop Produkt - SIA 380 / 2015 I - Basi per il calcolo energetico di edifici."

[18] "Welcome to LightGBM's documentation! — LightGBM 3.3.1.99 documentation." [Online]. Available: https://lightgbm.readthedocs.io/en/latest/

[19] "Optuna - A hyperparameter optimization framework." [Online]. Available: https://optuna.org/

[20] Y. Ozaki, Y. Tanigaki, S. Watanabe, and M. Onishi, "Multiobjective tree-structured parzen estimator for computationally expensive optimization problems," in *Proceedings of the 2020 Genetic and Evolutionary Computation Conference*, ser. GECCO '20. New York, NY, USA: Association for Computing Machinery, Jun. 2020, pp. 533–541. [Online]. Available: https://doi.org/10.1145/3377930.3389817

[21] D. S. Lee and T. Lemieux, "Regression Discontinuity Designs in Economics," *Journal of Economic Literature*, vol. 48, no. 2, pp. 281–355, Jun. 2010. [Online]. Available: https://pubs.aeaweb.org/doi/10.1257/jel.48.2.281

[22] "MoPEC." [Online]. Available: https://www.endk.ch/it/politica-energetica/mopec

[23] J. E. Martínez-Jaramillo, A. v. Ackere, and E. R. Larsen, "Transitioning towards a 100% solar-hydro based generation: A system dynamic approach," *Energy*, vol. 239, p. 122360, 2022. [Online]. Available: https://www.sciencedirect.com/science/article/pii/S0360544221026098

[24] M. Kubli and S. Ulli-Beer, "Decentralisation dynamics in energy systems: A generic simulation of network effects," *Energy Research & Social Science*, vol. 13, pp. 71–83, 2016. [Online]. Available: https://www.sciencedirect.com/science/article/pii/S2214629615300931

[25] R. Gupta, A. Pena-Bello, K. N. Streicher, C. Roduner, Y. Farhat, D. Thöni, M. K. Patel, and D. Parra, "Spatial analysis of distribution grid capacity and costs to enable massive deployment of PV, electric mobility and electric heating," *Applied Energy*, vol. 287, p. 116504, 2021. [Online]. Available: https://www.sciencedirect.com/science/article/pii/S0306261921000623

[26] "Electricity production plants." [Online]. Available: https://www.geocat.ch/geonetwork/srv/eng/catalog.search#/metadata/e5a00bdb-5022-4856-ad4a-d1afe7bf38b0

[27] "Suitability of roofs for solar power." [Online]. Available: https://www.geocat.ch/geonetwork/srv/eng/catalog.search#/metadata/b614de5c-2f12-4355-b2c9-7aef2c363ad6

[28] "RBD." [Online]. Available: https://www.geocat.ch/geonetwork/srv/eng/catalog.search#/metadata/56553efe-4a2c-449d-93ba-cf7edd518d56

[29] S. Cozza, M. K. Patel, and J. Chambers, "Uncertainty in potential savings from improving energy label: A Monte Carlo study of the Swiss residential buildings," *Energy and Buildings*, vol. 271, p. 112333, 2022. [Online]. Available: https://www.sciencedirect.com/science/article/pii/S0378778822005047

[30] S. Arzoyan, M. Vielle, Q. Oberpiller, and M. Zimmermann, Eds., *Endogenous Energy Efficiency Improvement of Large-Scale Refurbishment in the Swiss Residential Building Stock*, 2018.

[31] F. S. Office, "Federal Statistica Office." [Online]. Available: https://www.bfs.admin.ch/bfs/en/home/statistiken/bau-wohnungswesen/gebaeude.html

[32] ——, “Building size, FSO.” [Online]. Available: https://www.bfs.admin.ch/bfs/en/home/statistiken/bau-wohnungswesen/gebaeude/groesse.html

[33] S. Yilmaz, D. Majcen, M. Heidari, J. Mahmoodi, T. Brosch, and M. K. Patel, “Analysis of the impact of energy efficiency labelling and potential changes on electricity demand reduction of white goods using a stock model: The case of Switzerland,” *Applied Energy*, vol. 239, pp. 117–132, 2019. [Online]. Available: https://www.sciencedirect.com/science/article/pii/S030626191930203X

[34] “Standard di costruzione New Minergie.” [Online]. Available: https://www.minergie.ch/it/

[35] K. N. Streicher, P. Padey, D. Parra, M. C. Bürer, and M. K. Patel, “Assessment of the current thermal performance level of the Swiss residential building stock: Statistical analysis of energy performance certificates,” *Energy and Buildings*, vol. 178, pp. 360–378, 2018. [Online]. Available: https://www.sciencedirect.com/science/article/pii/S0378778818305875

[36] “Agent_based_model_solarpv.pdf.” [Online]. Available: https://www.psi.ch/sites/default/files/import/eem/PublicationsTabelle/Agent_based_model_solarPV.pdf

[37] J. Weniger, T. Tjaden, and V. Quaschning, “Sizing of Residential PV Battery Systems,” *Energy Procedia*, vol. 46, pp. 78–87, 2014. [Online]. Available: https://www.sciencedirect.com/science/article/pii/S1876610214001763

[38] M. Kubli and P. Canzi, “Business strategies for flexibility aggregators to steer clear of being “too small to bid”,” *Renewable and Sustainable Energy Reviews*, vol. 143, p. 110908, 2021. [Online]. Available: https://www.sciencedirect.com/science/article/pii/S136403212100201X

[39] ba!joodoo, “Karte: Typologie urbain-rural 2012,” tex.copyright: © Office fédéral de la statistique, ThemaKart, Neuchâtel 2009-#year#. [Online]. Available: https://www.atlas.bfs.admin.ch/maps/13/fr/17223_12361_3191_227/26733.html

[40] “Associazione professionale svizzera delle pompe di calore.” [Online]. Available: https://www.fws.ch/it/statistiche/

[41] S. F. O. o. E. SFOE, “Sector statistics.” [Online]. Available: https://www.bfe.admin.ch/bfe/en/home/versorgung/statistik-und-geodaten/energiestatistiken/teilstatistiken.html

[42] “Installations productrices de chaleur,” Mar. 2023. [Online]. Available: https://www.ge.ch/node/28193

[43] “Numero di occupanti per abitazione | Ufficio federale di statistica.” [Online]. Available: https://www.bfs.admin.ch/bfs/it/home/statistiche/costruzioni-abitazioni/abitazioni/condizioni-abitazione/densita-utilizzazione.html

[44] “Tariffe energia - Piano energetico cantonale (TICH) - Repubblica e Cantone Ticino.” [Online]. Available: https://www4.ti.ch/generale/piano-energetico-cantonale/fer/fondo-energie-rinnovabili-fer/tariffe-energia

[45] “Tarif de rétribution - pvtarif.ch La référence pour le tarif de rachat photovoltaique suisse.” [Online]. Available: https://www.vese.ch/wp-content/uploads/pvtarif/pvtarif2/appPvMapExpert/pvtarif-map-expert-fr.html?

[46] “Comune Bellinzona – Tariffe elettriche della Svizzera.” [Online]. Available: https://www.prezzi-elettricita.elcom.admin.ch/municipality/5002?period=2023&period=2022&period=2021&period=2020&period=2019&period=2018

[47] “JASM - Data platform - energy conversion technologies in STEM.” [Online]. Available: https://data.sccer-jasm.ch/

[48] “PdC-modulo di sistema - PdC-modulo di sistema - Pompe di calore efficienti con sistema.” [Online]. Available: https://www.wp-systemmodul.ch/files/

[49] "ME11_circulateurs_v1.1_annexe-1.pdf." [Online]. Available: https://media.sig-ge.ch/documents/sig/nous_connaitre/le_programme_eco_21/partenaire_eco21/ME11_Circulateurs_v1.1_Annexe-1.pdf

[50] p. Zürich, 8005, "Prezzo combustibili - proPellets," tex.copyright: © proPellets, Alle Rechte vorbehalten. [Online]. Available: https://www.propellets.ch/it/riscaldare-con-il-pellet/cifre-e-fatti/prezzo-del-pellet.html

[51] "Tariffario-fornitura-MSA-Validita-dal-01.10.2022.pdf." [Online]. Available: https://www.metanord.ch/wp-content/uploads/2022/08/Tariffario-fornitura-MSA-Validita-dal-01.10.2022.pdf

[52] S. Moret, "Strategic energy planning under uncertainty," phd, EPFL, 2017.

[53] "JASM - Data platform - energy conversion technologies in SES." [Online]. Available: https://data.sccer-jasm.ch/

[54] "TE_panoramica-incentivi.pdf." [Online]. Available: https://www.ticinoenergia.ch/docs/TE_panoramica-incentivi.pdf

[55] "Panneaux solaires thermiques | Genergie." [Online]. Available: https://www.ge-energie.ch/installation-solaire-thermique

[56] "Pompe à chaleur air-eau | Genergie." [Online]. Available: https://www.ge-energie.ch/pompe-chaleur-air-eau#

[57] "Programma d'incentivazione per riscaldamenti a pellet ecologici in Svizzera." [Online]. Available: https://www.myclimate.org/it/partecipare-attivamente/progetti-per-la-tutela-del-clima/dettagli-sui-progetti-di-protezione-del-clima/svizzera-biomassa-7822/

[58] "Live 24/7 CO emissions of electricity consumption." [Online]. Available: http://electricitymap.tmrow.co

[59] "RS 734.71 - Ordonnance du 14 mars 2008 sur l'approvisionnement en électricité (OApEl)." [Online]. Available: https://www.fedlex.admin.ch/eli/cc/2008/226/fr

[60] "Fondo energie rinnovabili (FER) - Piano energetico cantonale (TICH) - Repubblica e Cantone Ticino." [Online]. Available: https://www4.ti.ch/generale/piano-energetico-cantonale/fer/fondo-energie-rinnovabili-fer

[61] "Panneaux solaires photovoltaïques | Genergie." [Online]. Available: https://www.ge-energie.ch/installation-solaire-photovoltaique

[62] T. L. Bergman, F. P. Incropera, D. P. DeWitt, and A. S. Lavine, *Fundamentals of Heat and Mass Transfer*. John Wiley & Sons, Apr. 2011, google-Books-ID: vvyIoXEywMoC.

[63] T. Cholewa, M. Rosiński, Z. Spik, M. R. Dudzińska, and A. Siuta-Olcha, "On the heat transfer coefficients between heated/cooled radiant floor and room," *Energy and Buildings*, vol. 66, pp. 599–606, Nov. 2013. [Online]. Available: https://www.sciencedirect.com/science/article/pii/S0378778813004568

[64] L. S. Shieh, H. Wang, and R. E. Yates, "Discrete-continuous model conversion," *Applied Mathematical Modelling*, vol. 4, no. 6, pp. 449–455, Dec. 1980. [Online]. Available: https://www.sciencedirect.com/science/article/pii/0307904X80901778

# A Tables

| SFH | DFH | MFH |
|---|---|---|
| 1.15 | 1.2 | 1.2 |

Table 11: Correction factor by *Type* [35]

| | SFH | DFH | MFH |
|---|---|---|---|
| A | 1.9 | 1.4 | 1.4 |
| B | 2.4 | 2.1 | 2.1 |
| C | 2.8 | 2.6 | 2.6 |

Table 12: Occupants per dwelling by *Size* & *Type* [43]

| % | SFH | DFH | MFH |
|---|---|---|---|
| A | 63.85 | 53.61 | 73.87 |
| B | 78.47 | 77.83 | 76.54 |
| C | 82.9 | 85.93 | 89.22 |

Table 13: Share of suitable roofs [27]

| $m^2$ | SFH | DFH | MFH |
|---|---|---|---|
| A | 81.9 | 104.1 | 106.3 |
| B | 127.4 | 142.9 | 166.9 |
| C | 183 | 204.9 | 321.1 |

Table 14: Average roof size by *Size* and *Type* [28]

| $Rp/kWh$ | 2015 | 2016 | 2017 | 2018 | 2019 | 2020 | 2021 | 2022 | 2023 [2] |
|---|---|---|---|---|---|---|---|---|---|
| AMB [44] | 7.154 | 5.92 | 7.113 | 8.086 | 6.439 | 5.146 | 11.032 | 22.47 | 9.21 |
| GE [45] | 13.64 | 12 | 8.54 | 10.97 | 12.21 | 12.98 | 13.25 | 18.97 | 13.13 |

Table 15: Compensation for electricity sold to the grid

| $Rp/kWh$ | 2016 | 2017 | 2018 | 2019 | 2020 | 2021 | 2022 | 2023 |
|---|---|---|---|---|---|---|---|---|
| $e_p$ | 6.59 | 6.59 | 6.59 | 6.98 | 7.26 | 7.26 | 7.49 | 8.46 |
| $c_{TSO}$ | 1.56 | 1.56 | 1.56 | 1.56 | 1.56 | 1.56 | 1.56 | 1.56 |
| $c_{DSO}$ | 5.83 | 5.83 | 5.83 | 6.28 | 6.6 | 6.9 | 6.95 | 7.56 |
| $t_f$ | 2.3 | 2.3 | 2.3 | 2.3 | 2.3 | 2.3 | 2.3 | 2.3 |
| $t_c$ | 2.15 | 2.15 | 2.15 | 2.17 | 2.21 | 2.25 | 2.19 | 2.13 |
| $p$ | 18.43 | 18.43 | 18.43 | 19.29 | 19.93 | 20.27 | 20.49 | 21.9 |

Table 16: Electricity price in AMB serviced area [46]

[2] Computed as the average of the other years

| | Unit | Use | Oil Boiler | Gas Boiler | Wood Boiler | Pellet Boiler | ST | HP | EH | PV |
|---|---|---|---|---|---|---|---|---|---|---|
| Capital cost [47] | $CHF/kW$ | SFH<br>DFH/MFH | 1587<br>821 | 1460<br>756 | 2044<br>1764 | 2363<br>1764 | 8110<br>5661 | 2847<br>2180 | 730<br>378 | -<br>- |
| Annual fixed cost [47] | $CHF/kW/y$ | SFH<br>DFH/MFH | 10.22<br>41.09 | 10.22<br>37.8 | 21.27<br>88.2 | 42.54<br>88.2 | 405.51<br>283.07 | 8.54<br>109 | 10.22<br>18.9 | 28.8<br>28.8 |
| Lifetime [47] | $years$ | SFH<br>DFH/MFH | 15<br>20 | 15<br>20 | 15<br>25 | 15<br>25 | 15<br>15 | 15<br>20 | 15<br>15 | 30<br>30 |
| Efficiency [47] | - | SFH<br>DFH/MFH | 0.86<br>0.78 | 0.95<br>0.87 | 0.56<br>0.87 | 0.9<br>0.87 | 0.75<br>0.75 | 2.6<br>3.51 | 0.95<br>0.95 | -<br>- |
| Equivalent Hours [48] | $h/y$ | SH & DHW<br>Just SH | 2200<br>1900 | 2200<br>1900 | 2200<br>1900 | 2200<br>1900 | 2200<br>1900 | 2600 [49]<br>2200 | 2200<br>1900 | -<br>- |
| Carrier cost | $Rp/kWh_{th}$ | | 14.4 [50] | 16.2 [51] | 4.8 [52] | 13.8 [50] | - | Table 16 | Table 16 | Table 16 |
| GWP per Capacity [53] | $kg\,CO_2eq/kW$ | | 21.1 | 21.1 | 21.1 | 21.1 | 221.2 | 164.9 | 1.47 | 2081 |
| GWP variable [53] | $kg\,CO_2eq/MWh$ | | 331.5 | 267 | 11.8 | 11.8 | - | 117 [3] | 117 | -117 |
| Inv Grant (TI) | $CHF$ | | - | - | - | 5000 [54] | 2500 [54] | 7000 [54] | - | [4] |
| Inv Grant (GE) | $CHF$ | | - | - | - | - | 1200 [55] | 3000 [56] | - | [5] |
| Subsidy per Cap (TI) | $CHF/kW$ | | - | - | - | 100 [54] | 500 [54] | 180 [54] | - | [6] |
| Subsidy per Cap (GE) | $CHF/kW$ | | - | - | - | 360 [57] | 500 [55] | 400 [56] | - | [7] |

Table 17: Techno-economic parameters for the considered technologies

[3] The average emission form related to electricity from the grid is considered [58]

[4] There are two contributions, the federal one ("Remunerazione Unica" [59], 385 CHF + 420 CHF/kW) and the Cantonal one ("Contributo Unico" [60], 50 % of the "Remunerazione Unica")

[5] There are two contributions, the federal one ("Remunerazione Unica" [59], 385 CHF + 420 CHF/kW) and the Cantonal one ([61], 33 % of the "Remunerazione Unica")

[6] There are two contributions, the federal one ("Remunerazione Unica" [59], 385 CHF + 420 CHF/kW) and the Cantonal one ("Contributo Unico" [60], 50 % of the "Remunerazione Unica")

[7] There are two contributions, the federal one ("Remunerazione Unica" [59], 385 CHF + 420 CHF/kW) and the Cantonal one ([61], 33 % of the "Remunerazione Unica")

# B Avoided Costs

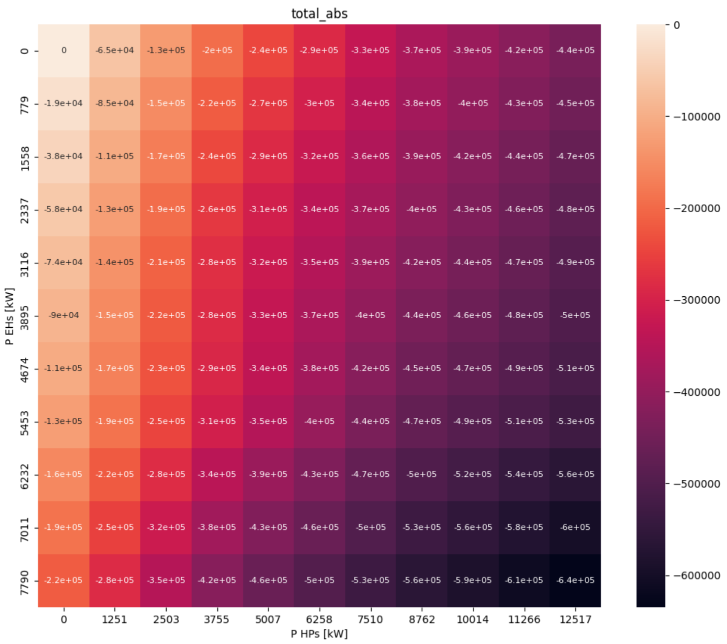


Figure 45: Total cost matrix for different combinations of total controlled HPs and electric boilers.

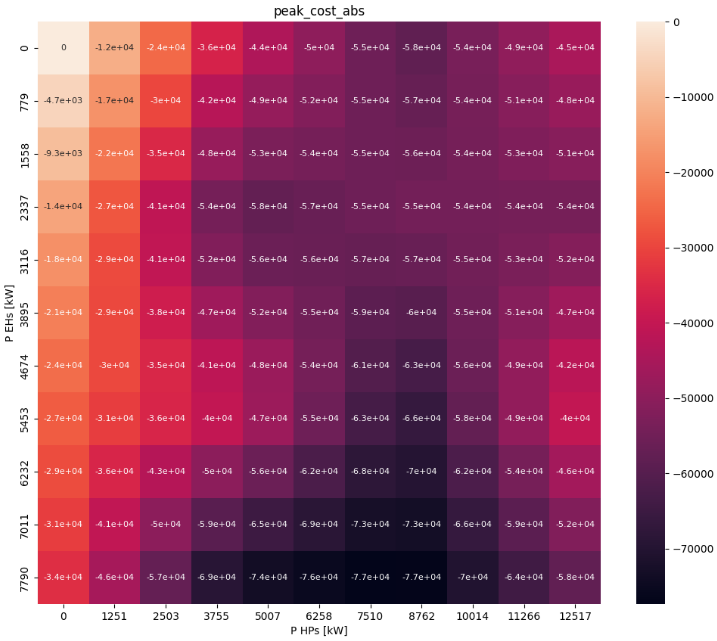


Figure 46: Peak cost matrix for different combinations of total controlled HPs and electric boilers.

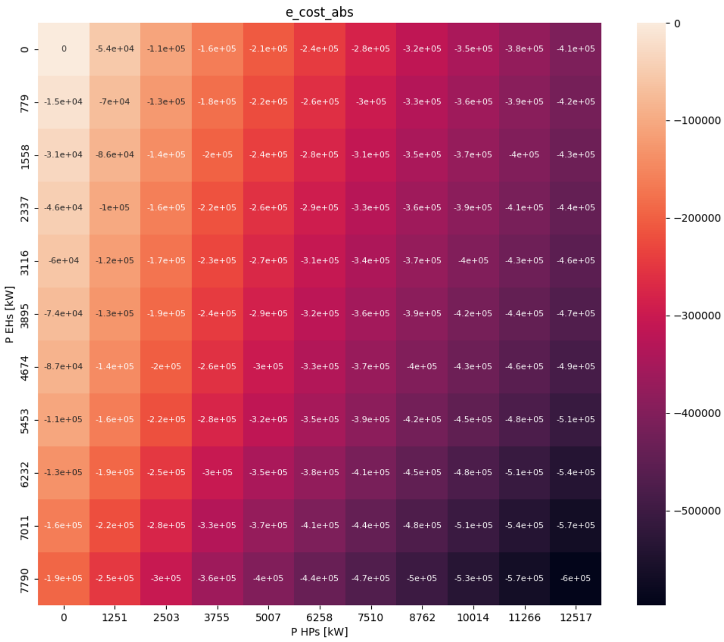


Figure 47: Energy cost matrix for different combinations of total controlled HPs and electric boilers.

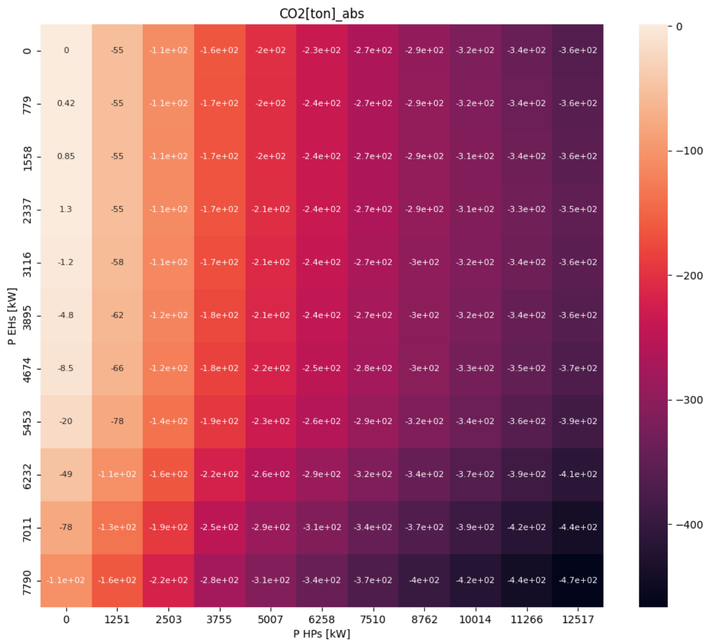


Figure 48: Avoided emission matrix for different combinations of total controlled HPs and electric boilers.

# C Thermal models

## C.1 Control logic of heating systems

The heat pump control logic is based on two temperature sensors placed at different heights of the water tank, while the circulation pump connecting the tank with the building's heating element is controlled by an hysteresis on the temperature measure by a sensor placed inside the house.

We describe the control logic in a sequential way, following the heating components of the system. The first decision is taken by the building central controller, which decides its working mode, that is, if the building needs to be cooled or heated, based on a moving average of the historical data of the external temperature:

$$\begin{cases} wm_t & = -1 \quad \textbf{if} \quad T_{ma,t} > T_{max,ma} \\ wm_t & = \;\; 1 \quad \textbf{if} \quad T_{ma,t} < T_{min,ma} \\ wm_t & = \;\; 0 \quad otherwise \end{cases} \tag{39}$$

where the working mode $wm_t$ is negative when the building requires to be cooled, positive when heating is required, and 0 when no actions are needed.$T_{max,ma}$ and $T_{min,ma}$ represent the maximum and minimum values of the external temperature's moving average, which is based on the past 7 days. The actual activation of the heating element is controlled by the hysteresis on the internal temperature of the building, $T_z$. If the working mode is positive, this is given by:

$$\begin{cases} s_{hy,t} & = 1 \quad \textbf{if} \quad (T_z < T_{min,hy} - \Delta T/2) \\ & \qquad \textbf{or} \quad (T_z < T_{min,hy} + \Delta T/2 \quad \textbf{and} \quad s_{hy,t-1}) \\ s_{hy} & = 0 \quad otherwise \end{cases} \tag{40}$$

where $s_{hy,t}$ is the state of the hysteresis at time $t$, 1 meaning that the circulation pump of the heating element must be activated, and $\Delta T$ was chosen to be equal to 1$^\circ C$. For completeness, we report also the control logic when the building is in cooling mode:

$$\begin{cases} s_{hy,t} & = 1 \quad \textbf{if} \quad (\,T_z > T_{max,hy} + \Delta T/2) \\ & \quad\quad\; \textbf{or} \quad (T_z > T_{max,hy} - \Delta T/2 \quad \textbf{and} \quad s_{hy,t-1}) \\ s_{hy} & = 0 \quad otherwise \end{cases} \tag{41}$$

The incoming water temperature in the heating element is then modulated linearly through a 3-way valve between a maximum and minimum value, based on the external temperature, both in the heating and cooling modes. When operative, the heating element requests hot or cold water to the water tank, which control logic is based on two temperature sensors located in two different layers. When the building is in heating mode, the control logic is a simple hysteresis based on the temperature of the sensor in the uppermost layer, which is identical to the one in (40). When in cooling mode, the control logic is the following:

$$\begin{cases} s_{hy,t} & = -1 \quad \textbf{if} \quad (\,T_{up} > T^c_{max} + \Delta T/2) \\ & \quad\quad\quad \textbf{or} \quad T_{low} > T^c_{max} + \Delta T/2 \\ s_{hy,t} & = 0 \quad\quad \textbf{if} \quad (\,T_{low} < T^c_{min}) \textbf{ or } (T_{up} < T^c_{max} - \Delta T/2) \\ s_{hy,t} & = s_{hy,t-1} \quad otherwise \end{cases} \tag{42}$$

where $T_{up}$ and $T_{low}$ are the temperature measured by the upper and lower sensors, respectively, and $T^c_{min}$ and $T^c_{max}$ are the minimum and maximum desired temperatures of the water in the tank while in cooling mode.
The value of $s_{hy,t}$ is then communicated to the HP. In the case in which the HP is also used for the domestic hot water (DHW), the DHW tank is always served with priority by the HP.

## C.2 Heat distribution system

Floor heating was modeled starting from first principles. Considering a fixed and uniform temperature for the ground and the building internal temperature at each time-step and stationary conditions, we can retrieve the analytical expression of the temperature profile along the pipe, through the energy balance on an infinitesimal element of the pipe. This can be expressed as:

$$\frac{\partial c T_x}{\partial t} = \Phi_x - \Phi_{x+\partial x} + \dot{q}_{up} + \dot{q}_{down} \tag{43}$$

where $c$ is the heat capacity in $J/K$, $x$ is the distance from the pipe entrance, $T_x$ is the temperature of the water inside the pipe at $x$, $\Phi$ are enthalpy flows at the entrance and exit of the considered infinitesimal volume, $\dot{q}_{up}$ and $\dot{q}_{down}$ are the heating powers from the building and from the ground. Expressing the latter through equivalent resistance taking into account convective and conductive effects, the balance in steady state can be rewritten as:

$$\frac{\dot{m} c_p}{\rho^*} \frac{\partial T_x}{\partial x} = \frac{R_{down} T_z + R_{up} T_g}{R_{down} + R_{up}} - T_x = T^a - T_x \tag{44}$$

where $T^a$ is the asymptotic temperature and where:

$$R_{down} = \frac{1}{h_{in} w} + \frac{1}{h_{u,eq} w} + R_u \tag{45}$$

$$R_{up} = \frac{1}{h_{in} w} + R_g \tag{46}$$

$$\rho^* = \frac{R_{up} + R_{down}}{R_{up} R_{down}} \tag{47}$$

where $w$ is the diameter of the tube, $h_{in}$ is the internal coefficient of heat transfer, which can be retrieved using available empirical relation for fully developed flow with fixed temperature at the boundary conditions [62], $h_{u,eq}$ is the heat transfer coefficient between the floor and the building air including both the effect for natural convection and radiation. The values of $h_{u,eq}$ can be found in the literature [63]. The value of the thermal resistances $R_u$ and $R_g$, towards the floor and the ground, can be found in the literature as well. We can reformulate (44), making it a-dimensional through a change of variable:

$$\frac{\partial \Theta}{\partial \mathcal{X}} = -\Theta \tag{48}$$

from which solution we can retrieve the temperature profile of the water inside the pipe:

$$T_x = T^a + (T_0 - T^a)e^{\frac{-x\rho^*}{\dot{m}c_p}} \tag{49}$$

where $T_0$ is the temperature of the water at the pipe inlet. We can use (49) to retrieve the heating power flowing into the building, integrating $\dot{q}_{up}(x)$ along the pipe.

$$\dot{Q}_{up} = \int_0^L \dot{q}_{up}(x)\mathrm{d}x = \int_0^L \frac{T(x) - T_z}{R_{up}}\mathrm{d}x \tag{50}$$

where $L$ is the length of the serpentine. Integrating, we obtain

$$\dot{Q}_{up} = \frac{(T^a - T_z)L - (T_L - T_0)\frac{\dot{m}c_p}{\rho^*}}{R_{up}} \tag{51}$$

where $T_L$ is the temperature of the water at the outlet of the serpentine. Note that the equation (51) tends to $(T_L - T_0)\dot{m}c_p$ when $R_{down}$ increase and $R_{up}$ is kept fixed.
The nominal mass flow of the heating system and the length of the serpentine are found as the solution of the following optimization problem:

$$\underset{L,\dot{m}}{\text{argmin}} \left(\dot{Q}_{up}(L) - \dot{Q}_{nom}\right)^2 + 10^{-3}\left(\dot{m} - \dot{m}_{nom}\right)^2 \tag{52}$$

where $\dot{m}_{nom}$ is a reference mass flow, equal to $0.1$ $[kg/s]$ and $\dot{Q}_{nom}$ is the power required to keep the building internal temperature constant under reference conditions (we used an external temperature of -4$°C$ and a desired internal temperature of 20 $°C$):

$$\dot{Q}_{nom} = \frac{\Delta T_{ref}}{R} \tag{53}$$

where $R$ is the resistance of an equivalent RC circuit describing the heating dynamics of the building.

## C.3 Water tank model

The dynamic equation describing the evolution of the temperature of the tank's layers is the following:

$$C\frac{\partial T_i}{\partial t} = \dot{Q}^u_{buo,i} + \dot{Q}^d_{buo,i} + \dot{Q}_{h,i} + \dot{Q}_{loss,i} + \dot{Q}^u_{cond,i} + \dot{Q}^d_{cond,i} + c_p\dot{m}(T_{i-1} - T_i) \tag{54}$$

where $T_i$ is the temperature of the $i_{th}$ layer, $Q^u_{buo}$,$Q^d_{buo}$,$Q^u_{cond}$,$Q^u_{cond}$ are the thermal powers due to buoyancy and conduction, from the lower and upper layer, respectively. The last term represents the enthalpy flow due to mass exchange, while $C$ is the thermal capacity of the layer, in $[J/K]$ and $Q_{h,i}$ is the thermal power due to an electric resistance (for the boiler) or an heat exchange (for the heating system buffer). The expression for the above thermal power are the following:

$$\dot{Q}^u_{buo,i} = k \max(T_{i+1} - T_i, 0)N, \quad 0 \quad for \quad i = N \tag{55}$$
$$\dot{Q}^d_{buo,i} = k \max(T_{i-1} - T_i, 0)N, \quad 0 \quad for \quad i = 1 \tag{56}$$
$$\dot{Q}^u_{cond,i} = u_{amb}(T_{i+1} - T_i), \quad 0 \quad for \quad i = N \tag{57}$$
$$\dot{Q}^d_{cond,i} = u_{amb}(T_{i-1} - T_i), \quad 0 \quad for \quad i = 1 \tag{58}$$
$$\dot{Q}_{loss,i} = u_{amb}(T_{ext} - T_i) \tag{59}$$
$$\dot{Q}_{h,i} = \dot{Q}_{tot}/n_h \quad if \quad i \in \mathcal{I} \tag{60}$$
$$\tag{61}$$

where $N$ is the number of layers, $u_{amb}$ is the equivalent thermal loss coefficient with the ambient and $\mathcal{I}$ is the set of the $n_h$ layers heated by the heat exchange (or electric resistance). The buoyancy model is the one proposed in the IDEAS library [3]. Detailed description of the parameters for the boiler model can be found in

## C.4 Fitting of equivalent thermal resistance

For each building we can solve the following optimization problem:

$$R^* = \underset{R}{\text{argmin}} \, (E_y - E_{sim}(\theta, R, T_{ext}, I))^2 \tag{62}$$

where $\theta$ are all the simulation's parameters, including the parameters for the heating system control logic. Solving this problem for all the buildings is impractical, since each evaluation of the objective function requires a yearly simulation for each building, which requires several minutes. As a first approximation, we can solve (62) replacing $E_{sim}$ with a proxy, $\tilde{E}$: instead of simulating the whole hating system and its logic, including stratified tanks, we can replace it with the following simplified equations:

$$q_{nom} = R^{-1}\Delta T_{ref} \tag{63}$$
$$u = T_{ma}(T_{ext}) < T_{ma,min} \tag{64}$$
$$q_{int,t} = q_{nom}(T_{t-1} < T_{min,t-1})u_t \tag{65}$$
$$T_t = T_{t-1}Ad + Bd(q_{int,t} + kI_t + T[t]R^{-1}) \tag{66}$$
$$\tilde{E}_{sim} = \sum_{t=1}^{t_{max}} q_{int,t} \tag{67}$$

where $\Delta T_{ref}$ is the reference temperature difference used for the sizing of the heating system, $T_{ma}$ is the one-week moving average on the external temperature, $T_{ma,min}$ indicates the value of $T_{ma}$ under which the heating is turned on, $u$ is a binary variable indicating if the heating system is active, $T_{min}$ is the time-dependent vector of minimum internal temperatures, $Ad$ and $Bd$ are the exactly discretized dynamic matrices, obtained by the continuous one through exact discretization [64]:

$$\begin{aligned} A_d &= e^{A_c dt} \\ B_d &= A_c^{-1}(A_d - I)B_c \end{aligned} \tag{68}$$

where $A_c = [-\frac{1}{RC}]$ and $B_c = [-\frac{1}{C}]$. Equations (63)-(67) allows to reduce the computational cost for a yearly simulation with 10 minutes sampling time for one building down to 0.5 milliseconds on average, when compiled with numba, making it practical to solve (62) through gradient-based optimization for all the simulated buildings.